NAVAL POSTGRADUATE SCHOOL
Monterey, California

THESIS

COAMPS MODELED SURFACE LAYER REFRACTIVITY IN THE ROUGHNESS AND EVAPORATION DUCT EXPERIMENT 2001

by

D. Adam Newton

June 2003

Thesis Advisor: K. Davidson
Co-Advisor: D. Miller

Approved for public release; distribution is unlimited.

THIS PAGE INTENTIONALLY LEFT BLANK

REPORT DOCUMENTATION PAGE			Form Approved OMB No. 0704-0188
Public reporting burden for this collection of information is estimated to average 1 hour per response, including the time for reviewing instruction, searching existing data sources, gathering and maintaining the data needed, and completing and reviewing the collection of information. Send comments regarding this burden estimate or any other aspect of this collection of information, including suggestions for reducing this burden, to Washington headquarters Services, Directorate for Information Operations and Reports, 1215 Jefferson Davis Highway, Suite 1204, Arlington, VA 22202-4302, and to the Office of Management and Budget, Paperwork Reduction Project (0704-0188) Washington DC 20503.			
1. AGENCY USE ONLY ***(Leave blank)***	**2. REPORT DATE** June 2003	**3. REPORT TYPE AND DATES COVERED** Master's Thesis	
4. TITLE AND SUBTITLE: COAMPS Modeled Surface Layer Refractivity in the Roughness and Evaporation Duct Experiment 2001			**5. FUNDING NUMBERS**
6. AUTHOR(S) LT D. Adam Newton			
7. PERFORMING ORGANIZATION NAME(S) AND ADDRESS(ES) Naval Postgraduate School Monterey, CA 93943-5000			**8. PERFORMING ORGANIZATION REPORT NUMBER**
9. SPONSORING /MONITORING AGENCY NAME(S) AND ADDRESS(ES) N/A			**10. SPONSORING/MONITORING AGENCY REPORT NUMBER**
11. SUPPLEMENTARY NOTES The views expressed in this thesis are those of the author and do not reflect the official policy or position of the Department of Defense or the U.S. Government.			
12a. DISTRIBUTION / AVAILABILITY STATEMENT Approved for public release; distribution is unlimited.			**12b. DISTRIBUTION CODE**

13. ABSTRACT ***(maximum 200 words)***

A study of the performance of the Coupled Ocean Atmosphere Mesoscale Prediction System (COAMPS) was performed based on collected METOC properties affecting radar propagation during the Roughness and Evaporation Duct (RED) experiment conducted off the windward coast of Oahu, HI. The measured refractivity influencing parameters (SST, air temperature, humidity, and wind speed) were compared to COAMPS predicted values. Using the NPS bulk evaporation duct model, profiles of the modified refractivity were computed from the buoy data and compared to profiles computed from the COAMPS data. The profiles were obtained concurrently with S-Band propagation measurements along a 26-km path. The radar propagation predictions created by APM from the modified refractivity profiles, derived from the measured METOC values and COAMPS modeled values, were compared to the in situ measured propagation losses. The mean RMS error of the prop loss predictions derived from the COAMPS forecasted METOC values was <4 dB compared to a mean RMS error of <3 dB from the in situ measurement derived prop loss predictions. Significantly larger errors occurred at the COAMPS analysis times. Overall, the results are very promising for this trade wind region, where the air is cooler than the relatively warm sea surface.

14. SUBJECT TERMS Rf propagation, boundary layer, refractivity, bulk, COAMPS, APM, RED, evaporation duct			**15. NUMBER OF PAGES** 76
			16. PRICE CODE
17. SECURITY CLASSIFICATION OF REPORT Unclassified	**18. SECURITY CLASSIFICATION OF THIS PAGE** Unclassified	**19. SECURITY CLASSIFICATION OF ABSTRACT** Unclassified	**20. LIMITATION OF ABSTRACT** UL

NSN 7540-01-280-5500 Standard Form 298 (Rev. 2-89)
Prescribed by ANSI Std. 239-18

THIS PAGE INTENTIONALLY LEFT BLANK

Approved for public release; distribution is unlimited.

COAMPS MODELED SURFACE LAYER REFRACTIVITY AT THE ROUGHNESS AND EVAPORATION DUCT EXPIREMENT 2001

D. Adam Newton
Lieutenant, United States Navy
B.A., University of San Diego, 1995

Submitted in partial fulfillment of the
requirements for the degree of

**MASTER OF SCIENCE IN
METEOROLOGY AND PHYSICAL OCEANOGRAPHY**

from the

**NAVAL POSTGRADUATE SCHOOL
June 2003**

Author:

D. Adam Newton

Approved by:

Kenneth Davidson
Thesis Advisor

Douglas Miller
Co-advisor

Carlyle Wash, Chairman
Department of Meteorology

THIS PAGE INTENTIONALLY LEFT BLANK

ABSTRACT

A study of the performance of the Coupled Ocean-Atmosphere Mesoscale Prediction System (COAMPS) was performed based on collected METOC properties affecting radar propagation during the Roughness and Evaporation Duct (RED) experiment conducted off the windward coast of Oahu, HI. The measured refractivity influencing parameters (SST, air temperature, humidity, and wind speed) were compared to COAMPS predicted values. Using the NPS bulk evaporation duct model, profiles of the modified refractivity were computed from the buoy data and compared to profiles computed from the COAMPS data. The profiles were obtained concurrently with S-Band propagation measurements along a 26-km path. The radar propagation predictions created by APM from the modified refractivity profiles, derived from the measured METOC values and COAMPS modeled values, were compared to the in situ measured propagation losses. The mean RMS error of the prop loss predictions derived from the COAMPS forecasted METOC values was <4 dB compared to a mean RMS error of <3 dB from the in situ measurement derived prop loss predictions. Significantly larger errors occurred at the COAMPS analysis times. Overall, the results are very promising for this trade wind region, where the air is cooler than the relatively warm sea surface.

THIS PAGE INTENTIONALLY LEFT BLANK

TABLE OF CONTENTS

THIS PAGE INTENTIONALLY LEFT BLANK

LIST OF FIGURES

ACKNOWLEDGMENTS

I'd like to thank the people and agencies without whom this thesis could never have been completed. For RED data and results, Paul Frederickson supported the numerous NPS bulk model and APM calculations and Kenn Anderson of Spawar Systems Center San Diego provided the propagation loss data. For the COAMPS data, Dr. Jeff Reid, Naval Research Laboratory, Monterey, arranged for the COAMPS predictions, and Dr. Peter Caffrey and Dr. Roger Shi, Naval Research Laboratory, Washington, DC for provided the COAMPS predictions. Robert Crease and Tamar Neta of NPS supported the formatting of COAMPS data into a usable form. Without all this help, I could not have accomplished this. The ONR Marine Meteorology Program (code 322MM) and SPAWAR (PMW-155) made funding for this work possible.

THIS PAGE INTENTIONALLY LEFT BLANK

I. REQUIREMENTS AND IMPORTANCE OF MODIFIED REFRACTIVITY IN THE SURFACE LAYER

A. INTRODUCTION

This study is an investigation the feasibility of using model forecast fields to create radar propagation forecasts. Specifically, it is a study of the value of propagation predictions derived from the NPS bulk evaporation duct model using METOC input values from the Navy's Coupled Ocean-Atmosphere Mesoscale Prediction System (COAMPS) model forecasts. The value of the propagation forecasts are based on comparisons with similar propagation predictions based on in-situ measurements and verified against actual propagation measurements.

A Mobile Environmental Team embarked on the USS PORT ROYAL examined methods of integrating the METOC and Surface Warfare battle spaces. A report by CAPT Easton and LT Sanabia, titled "Exploiting the Environment to Win in the 21st Century," resulted (Easton and Sanabia 2000). This 'White Paper' stressed the need to inject METOC considerations into the tactical picture to optimize sensor coverage for the current environment, and predicted future environmental conditions to benefit operational decision-making. An important recommendation was to create a joint SWO/METOC technology package in which combat systems algorithms and atmospheric assessment/predictive tools include environmental conditions and radar specifications that are fully compatible. This technology package would consist of components to a) determine what the current atmospheric conditions are; b) assess how the environmental conditions affect radar detection of various threats; c) recommend radar settings to optimize sensor coverage for the current environment; and d) predict future environments and their effects on sensors.

The motivation for all of this is that knowledge of radio frequency (Rf) propagation properties near the sea surface is required to assess/predict the radar detection of a wide range of threats, particularly low-flying planes or missiles, and small boats. Near the sea surface Rf propagation is controlled by the existence, height, and strength of evaporation and surface-based ducts. Therefore, accurate knowledge of these

refractivity features is critical to predicting the radar detection of specific threats and to optimize radar coverage for the given environmental conditions.

Electromagnetic (EM) waves propagate along curved paths through the atmosphere due to spatial variations in temperature and humidity. The vertical gradients of these properties are especially strong near the earth's surface, which can lead to highly anomalous propagation conditions. For example, the rapid decrease of humidity with height normally occurring just above the ocean surface often results in refractive conditions that cause radio frequency waves to bend downward toward the earth's surface and to become channeled within a thin layer. This refractive feature is known as an 'evaporation duct'. Radio waves propagating within an evaporation duct may travel well beyond normally expected distances and with greater-than-expected field strength.

Evaporation ducts are present with varying characteristics most of the time in every oceanic region of the world. Therefore, knowledge of the presence, height and strength of evaporation ducts is critical to properly assess and predict the near-horizon propagation of radio frequency waves over the ocean surface. The phenomenon of evaporative ducting and the ability to predict its effects has obvious implications for maritime communications and navigation, radar meteorology, and naval activities such as electronic counter-measures and the radar detection and tracking of low-flying missiles and aircraft, surface combatants and submarine periscopes.

It is not feasible to directly measure the evaporation duct from operational platforms at sea, since this requires measurements of temperature and humidity at closely spaced height levels just above the sea surface with very high accuracy. The obvious difficulties encountered in obtaining such sensitive vertical profile measurements from a pitching and rolling ship at sea and the problems of flow-distortion and thermal contamination caused by the ship's hull and superstructure, not to mention maintaining sensor accuracy in the rugged marine environment with constant exposure to salt water spray, make it doubtful that the direct measurement of evaporation ducts from shipboard sensors will be operationally possible in the near future.

Current atmospheric profiling techniques, such as balloon-ascending radiosondes and parachute-descending rocketsondes, generally do not measure close enough to the

ocean surface and have neither the vertical resolution nor the rapid sensor response and accuracy required to adequately describe the evaporation duct. Such profile measurements represent only a single sounding through the turbulent lower atmosphere, which is often characterized by intermittent convective cells where an ensemble average of multiple soundings is required to adequately describe the vertical structure of the atmosphere. Additionally, these sounding techniques are not continuous in time, are expensive to perform operationally and may reveal the presence of the parties conducting the measurements, which may be undesirable in naval applications

The need to understand Rf propagation conditions from the surface through the boundary layer capping inversion (normally 2,000-4,000 feet) has been recognized for several years, and has led to the development and prospective deployment of numerous METOC measurement and processing systems, including MORIAH (SMOOS(R)), TDrop, Lidar, GBHIS and SPY-1 TEP. Furthermore, it has led to the formulation of methods for interpreting multi-spectral data obtained from satellite-borne sensors. Along with the improved methods of obtaining observational data have come physical models for applying them.

Due to the difficulties discussed above in directly measuring the evaporation duct, so-called 'bulk' models have been used to estimate the near-surface refractivity conditions over the ocean for several decades (e.g. Fairall et al. 1978, Patterson 1985, Paulus 1985, Babin et al. 1997). Bulk surface layer models require as inputs mean measurements of wind speed, temperature, humidity and pressure obtained at a single height level above the surface within the atmospheric boundary layer (ABL; assumed to be from the surface to 50m) and the ocean surface temperature. Such measurements can be continuously obtained from ships, buoys and ocean towers relatively easily, although care does need to be taken to reduce the effects of flow distortion, thermal contamination, and sensor exposure to the maritime environment. Near-surface refractivity profiles can be estimated from bulk models and directly input into EM propagation assessment models using Monin-Obukhov similarity (MOS) theory and existing ocean surface parameterizations.

The Naval Postgraduate School (NPS) has developed an operational near-surface refractivity model (Frederickson and Davidson 2003) which computes near-surface refractivity profiles and the evaporation duct height from environmental measurements provided by the shipboard SMOOS(R) measurement system. The model refractivity profiles can then be input into propagation assessment programs such as AREPS to predict near-surface radar performance in the current environment, including the probability of detection of specific threats.

The prediction requirement arises from the need to understand spatial as well as temporal variations in refractive conditions to properly assess Rf propagation and threat detection in the tactical battle space. Studies have shown that assumptions of horizontal homogeneity can lead to large propagation assessment errors in a spatially varying atmosphere (Goldhirsh and Dockery, 1994).

The Roughness and Evaporation Duct (RED) experiment conducted off the windward coast of Oahu in 2001 provided an ideal data set for evaluating the value of COAMPS prediction and for testing the study's methodology. In RED, radar propagation measurements were obtained over a 26 km path between a moored platform (RP FLIP) and a shore station. Concurrent METOC measurements were obtained from the NPS "Flux" buoy in the vicinity of the 26-km path. The buoy METOC data were input into the Naval Postgraduate School's (NPS) bulk evaporation duct model to compute a refractivity profile, which was then used to run the Advanced Propagation Model (APM) to obtain propagation loss values.

COAMPS-predicted near surface values of wind speed, air and sea temperature, humidity and pressure were averaged over several grid points in the RED propagation path area and were then input into the NPS bulk model and then the APM to compute propagation loss predictions. These COAMPS-derived propagation loss predictions were then compared with the flux buoy-derived values and the actual propagation measurements. This study will be the first in which the mesoscale prediction is addressed and will examine the integration of data and models required for the optimization of sensor coverage.

B. BACKGROUND

1. Modified Refractivity and Ducting Layers

The propagation of EM radiation through the atmosphere is determined by the vertical and horizontal gradients of the refractive index of air, *n*, defined as the ratio of the speed of a radar (EM) wave front through a vacuum over the speed through air. EM waves bend or 'refract' toward regions of higher *n*. Because *n* is so close to one, the 'refractivity', *N*, which describes the difference of *n* from one, is often used. For microwave and millimeter-wave radiation (roughly 100 MHz – 100 GHz), *N* is related to the atmospheric variables of absolute temperature (*T*), partial pressure of water vapor (*e*) and total atmospheric pressure (*P*) through the following equation (Bean and Dutton 1968):

$$N = (n-1)\times 10^6 = 77.6\frac{P}{T} - 5.6\frac{e}{T} + 3.75\times 10^5 \frac{e}{T^2}, \qquad (1)$$

where *T* is in K, and *P* and *e* are in hPa.

For determining the presence or absence of ducts and trapping layers in the atmosphere a quantity called the 'modified refractivity', M, is used which takes the curvature of the earth's surface into account, as follows:

$$M = N + \frac{z}{r_e \times 10^{-6}} = N + 0.1568\ z, \qquad (2)$$

where r_e is the earth's radius (≈ 6.378×10^6 m), *z* is the height above the surface, both expressed in meters. It is the vertical gradient of *m* (d*m*/dz), rather than its absolute value, that determines the presence of ducts. When d*m*/dz = 0, the EM ray curvature is equal to the earth's curvature and propagating waves travel parallel to the earth's surface; when d*m*/dz > 0, EM rays curve upward relative to the earth's surface; when d*m*/dz < 0, EM rays curve downward relative to the earth's surface. If a negative d*m*/dz layer extends down to the surface, then EM rays can be trapped between the reflecting sea surface and the top of the layer and a phenomenon known as 'ducting' occurs.

To form the negative vertical *m* gradient required for a surface-based duct, the air temperature must increase rapidly with height and/or the vapor pressure must decrease

rapidly with height just above the surface. Since the humidity over the ocean generally decreases rapidly with height above a near-saturation humidity value at the surface, a thin surface-based duct usually exists over the ocean. Such ducts have historically been given the name 'evaporation ducts' because the humidity profile leading to the formation of the duct is associated with evaporation from the ocean surface.

The top of the duct in such a situation is referred to as the 'evaporation duct height' (EDH) and is located where dm/dz = 0, i.e. the height of the local minimum in m nearest the surface. The region where dm/dz < 0 is known as a "trapping layer". The trapping layer between the surface and the evaporation duct height acts like a simple 'wave guide' for channeling EM waves. Waves propagating near the ocean surface, especially those within the trapping layer, may travel over much greater distances and with much greater field strength than normally expected. Relative to radar performance, the existence of this trapping layer causes increased clutter, which is the primary concern when setting the sensitivity of the radar. For this reason information on the presence and height of the evaporation duct is critical to properly assess EM propagation near the ocean surface.

2. Monin-Obukhov Similarity (MOS) Theory Overview

Monin-Obukhov similarity (MOS) theory provides a powerful tool for estimating the near-surface refractivity profiles and the characteristics of the evaporation ducts from mean meteorological measurements obtained at a single level in the atmosphere and at the surface. According to MOS theory, conditions are assumed to be horizontally homogeneous and stationary and the turbulent fluxes of momentum, sensible heat and latent heat are assumed to be constant with height in what is referred to as the "atmospheric surface layer." Surface-layer scaling parameters for wind speed u_*, potential temperature, θ_*, and specific humidity, q_*, are defined in terms of the assumed-constant kinematic fluxes, as follows:

$$u_* \equiv (-\overline{w'u'})^{1/2}, \tag{3a}$$

$$\theta_* \equiv -\frac{\overline{w'\theta'}}{u_*}, \tag{3b}$$

$$q_* \equiv -\frac{\overline{w'q'}}{u_*}, \qquad (3c)$$

where the primed quantities represent the turbulent fluctuations of the streamwise wind component (u), the vertical wind component (w), potential temperature (θ), and specific humidity (q), and the overbar denotes an ensemble average. Near the surface we can define the potential temperature as $\theta \approx T + \Gamma_d \times z$, where T is the air temperature, Γ_d is the dry adiabatic lapse rate (≈ 0.00976 K m^{-1}) and z is the height above the surface.

According to MOS theory, all dynamic properties in the surface layer are assumed to depend only upon the height above the surface (z), the buoyancy parameter $(g/\theta)_v$ (where g is the gravitational acceleration and θ_v is the virtual potential temperature), and the scaling parameters u_*, θ_* and q_*. These five parameters can be combined to form the dimensionless ratio ξ, defined as:

$$\xi = \frac{z}{L} = \frac{zkg\left[\theta_*\left(1+0.6078q\right)+0.6078Tq_*\right]}{\theta_v u_*^2}, \qquad (4)$$

where L is the Obukhov length scale and k is the von Karman constant (= 0.4). The ratio ξ is often referred to simply as the 'stability', and is negative in unstable conditions; zero in neutral conditions, and positive in stable conditions. When MOS theory is valid, any dynamic surface-layer property made dimensionless by normalizing with the scaling parameters z, g/θ_v, u_*, θ_* and q_*, can be expressed as a universal function of ξ alone. The vertical profiles of wind speed (U), potential temperature (θ) and specific humidity (q) have been found to follow MOS theory well within the surface layer under a wide range of conditions.

3. Near-Surface Profile and Evaporation Duct Height Determination

At the core of the NPS evaporation duct model is a slightly modified form of the TOGA-COARE bulk model version 2.6. This model is widely used within the boundary layer community and has been verified in numerous field experiments. The TOGA-COARE model is used to determine the surface layer scaling parameters. Once the bulk surface-layer model has produced estimates of the scaling parameters, the near-surface

profiles of temperature and specific humidity are computed from the following equations, which are a function of z:

$$T(z) = T_{sea} + \frac{\theta_*}{k}\left[\ln\left(\frac{z}{z_{o\theta}}\right) - \Psi_\theta\left(\frac{z}{L}\right)\right] - \Gamma_d z \quad , \qquad (5a)$$

$$q(z) = q_{sea} + \frac{q_*}{k}\left[\ln\left(\frac{z}{z_{o\theta}}\right) - \Psi_\theta\left(\frac{z}{L}\right)\right] \quad , \qquad (5b)$$

where T_{sea} is the measured mean value of the sea surface temperature and q_{sea} = $0.98q_{sat}(T_{sea})$, as discussed above. The saturation specific humidity (q_{sat},) is computed from temperature using the saturation vapor pressure equation presented by Buck (1981).

The profile of atmospheric pressure is determined by combining the hydrostatic equation and the ideal gas law and integrating, resulting in the hypsometric equation:

$$P(z_2) = P(z_1)\exp\left(\frac{g(z_1 - z_2)}{R\overline{T_v}}\right) \quad , \qquad (6)$$

where R is the ideal gas law constant for dry air (= 287.04 J kg^{-1} K^{-1}) and $\overline{T_v}$ is the mean virtual temperature in the layer between heights z_1 and z_2, determined by the simple average $\overline{T_v} = \left[T_v(z_1) + T_v(z_2)\right]/2$.

The partial pressure of water vapor (e), which is required to compute the desired quantity of modified refractivity, can be computed from the specific humidity by the expression:

$$e = \frac{qP}{\varepsilon + (1-\varepsilon)q} \quad , \qquad (7)$$

where ε is the ratio of the gas constants for dry air over that of water vapor (= 0.62197). The physical constant values and meteorological equations used in the model are described in Goroch et al. (2000).

Once profiles of T, e and P have been determined from Eqs. (5-7), the vertical modified refractivity (m) profile can be computed from Eqs. (1-2). The evaporation duct height, z_{duct}, is determined from the computed m profile by finding the height closest to

the surface where both dm/dz = 0 and a local minimum in m occurs. Since the bulk evaporation duct model is based on MOS theory, it is only valid within the atmospheric surface layer where the vertical profiles of T and q depend only upon the surface layer scaling parameters and the turbulent fluxes are nearly constant with height.

4. Operational Features of the NPS Evaporation Duct Model

The required model input parameters are time-averaged values of the wind speed, air temperature, relative humidity and barometric pressure obtained at a single height within the atmospheric surface layer; and sea surface temperature. In addition, the heights above the surface at which all the atmospheric measurements were obtained must be known and input into the model. All of the atmospheric measurements (wind speed, air temperature, humidity and pressure) required as inputs to the model can be obtained at any height within the atmospheric surface layer and all four of these atmospheric parameters can be measured at different heights. Great effort should be made to minimize the effects of flow distortion and thermal contamination on the measurements caused by poor measurement platform positioning, if at all possible. The input values should be averaged over a minimum interval of 5 minutes, with a 10-minute minimum interval being preferable.

C. EVAPORATION DUCT IMPACT ON NAVAL APPLICATIONS

An operational illustration of the prediction requirement to obtain appropriate data is demonstrated in Figure 1, which shows 24-hour time series of continually measured METOC parameters from the USS ANZIO and USS CAPE ST. GEORGE, deployed in the Persian Gulf (Davidson 2002). The top panel shows how the separation of the two ships varied (the black line). These time series were obtained with the SEAWASP/ SMOOS(R) system that is being installed on combatant ships to meet measurement requirements. In the time series, the vertical refractive profile is indicated by the evaporation duct height (EDH) titled “Duct” in the lowest panel. The EDH is calculated from the other METOC variables. The evaporation duct height values (10 to 30 meters) span a significant effect range relative to the SPY-1 radar performance. Between 04Z and 06Z the duct height difference between the CAPE ST. GEORGE and ANZIO increases significantly due to position changes only. The CAPE ST. GEORGE steamed

northwestward during this time. The change in duct height was due to a drop in RH, which was the result of the CAPE ST. GEORGE and ANZIO being on opposite sides of a front.

M profiles for the ANZIO and CAPE ST. GEORGE at 04Z and 06Z are shown in Figure 2. It is clear that the EDH is not a distinct feature in the profile and that these M profiles were not measured directly; they were calculated from the measured METOC parameters (at most one height in the air and the SST). These calculations must be based on models that include mixing processes that determine the gradients above and below the measurement level, from the surface to above 30-40 m.

This realization along with the forecast issue has led to continuing Navy atmospheric modeling efforts to assess and predict mesoscale conditions. Having the capability to operationally predict atmospheric effects on sensors and weapons systems for a region of interest would improve the U.S. Navy's tactical decision making allowing commanders to position their assets in order to optimize force protection or strike effectiveness based on the future propagation conditions in the tactical battle space. It is believed shipboard METOC propagation assessment and mesoscale modeling can both greatly benefit by being operationally linked to each other.

The effect of evaporation ducting is dependent on frequency. Figure 3 shows propagation loss for L-Band, S-Band, X-Band and Ku-Band frequencies for an evaporation duct height of 20 meters and an antenna height of 10 meters. The L-Band frequency (1 GHz) is relatively unaffected by evaporation ducting. The S-Band frequency (3 GHz) shows extended ranges at all heights, but especially near the evaporation duct height. The X-Band frequency (10 GHz) exhibits decreased propagation loss centered on the antenna height while the Ku-Band frequency (18 GHz) shows decreased loss near the antenna height as well as near the evaporation duct height. These results are specific to the environment, antenna height and frequencies used, but do serve to illustrate the frequency-dependent nature of propagation in the presence of an evaporation duct.

The SPY-1A, B, B(V), D and D(V) radars all use S-Band frequencies, and future generations of the SPY radar may operate at even higher frequencies. To take full

advantage of the capabilities of the SPY-1 radar, operators must account for changing near-surface refractivity conditions (Easton and Sanabia 2000). Therefore, this thesis will concentrate on the S-Band, although X-Band and Ku-Band radars were also measured.

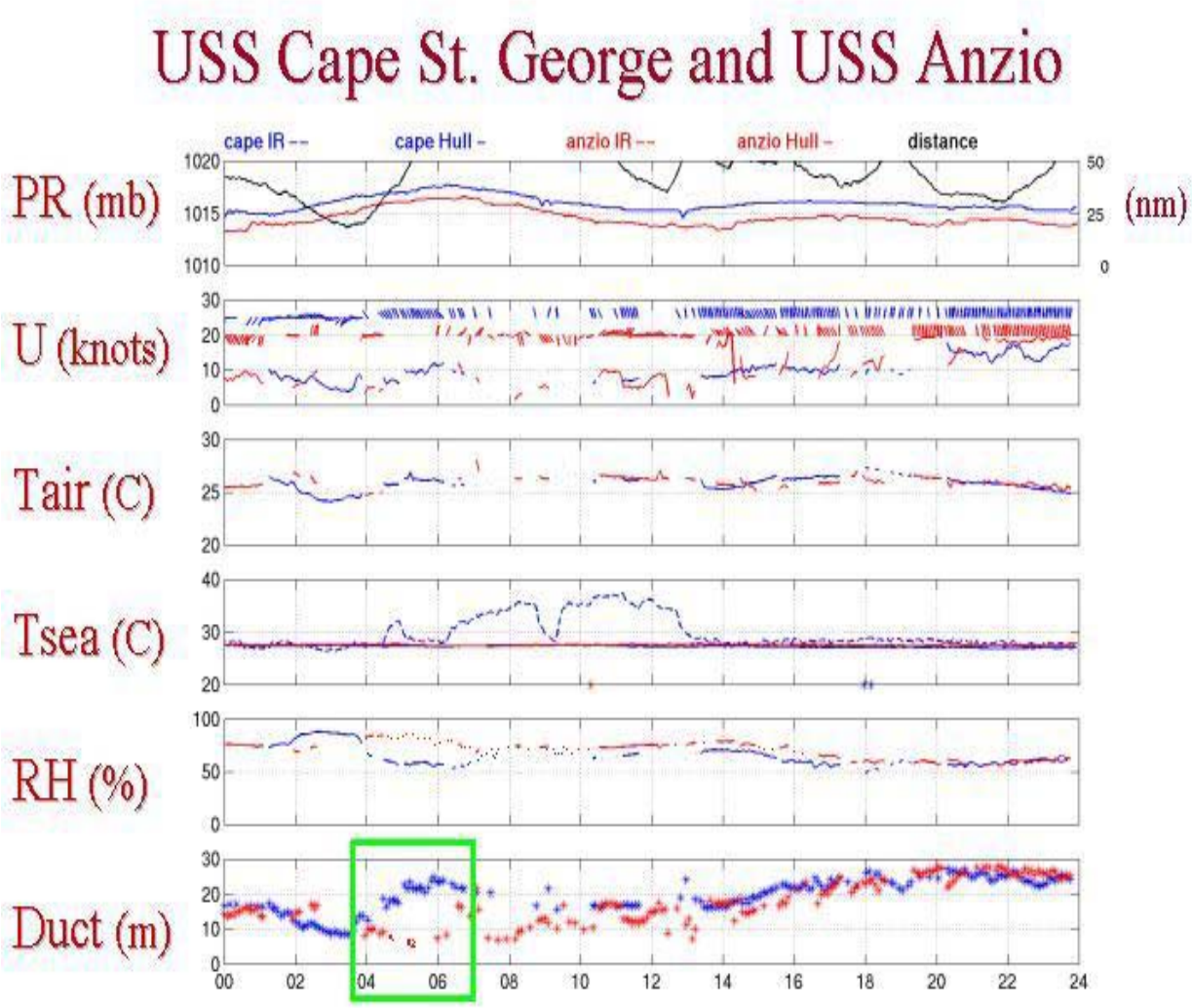

Figure 1. 24-hour time series of Pressure, WS, Tair, SST, RH and EDH recorded onboard the USS ANZIO (red) and USS CAPE ST. GEORGE (blue) and the distance between the two ships (black). The green box highlights the time period during which the two ships are on different sides of a front, impacting the RH and, therefore the EDH.

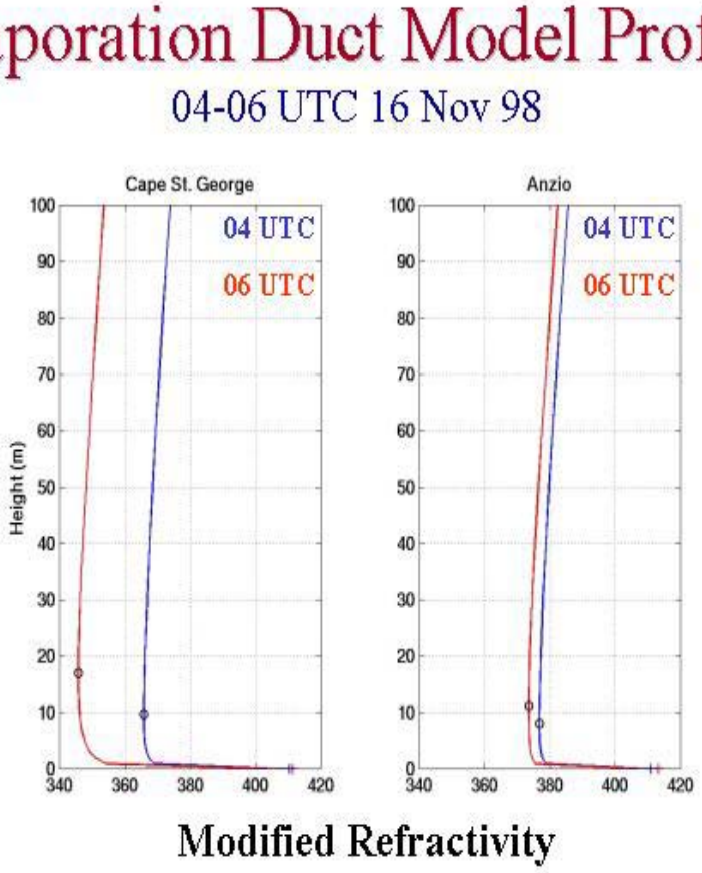

Figure 2. M profiles for the USS CAPE ST. GEORGE (left) and USS ANZIO (right), at 04Z (blue) and 06Z (red) computed from the METOC values depicted in Figure 1.

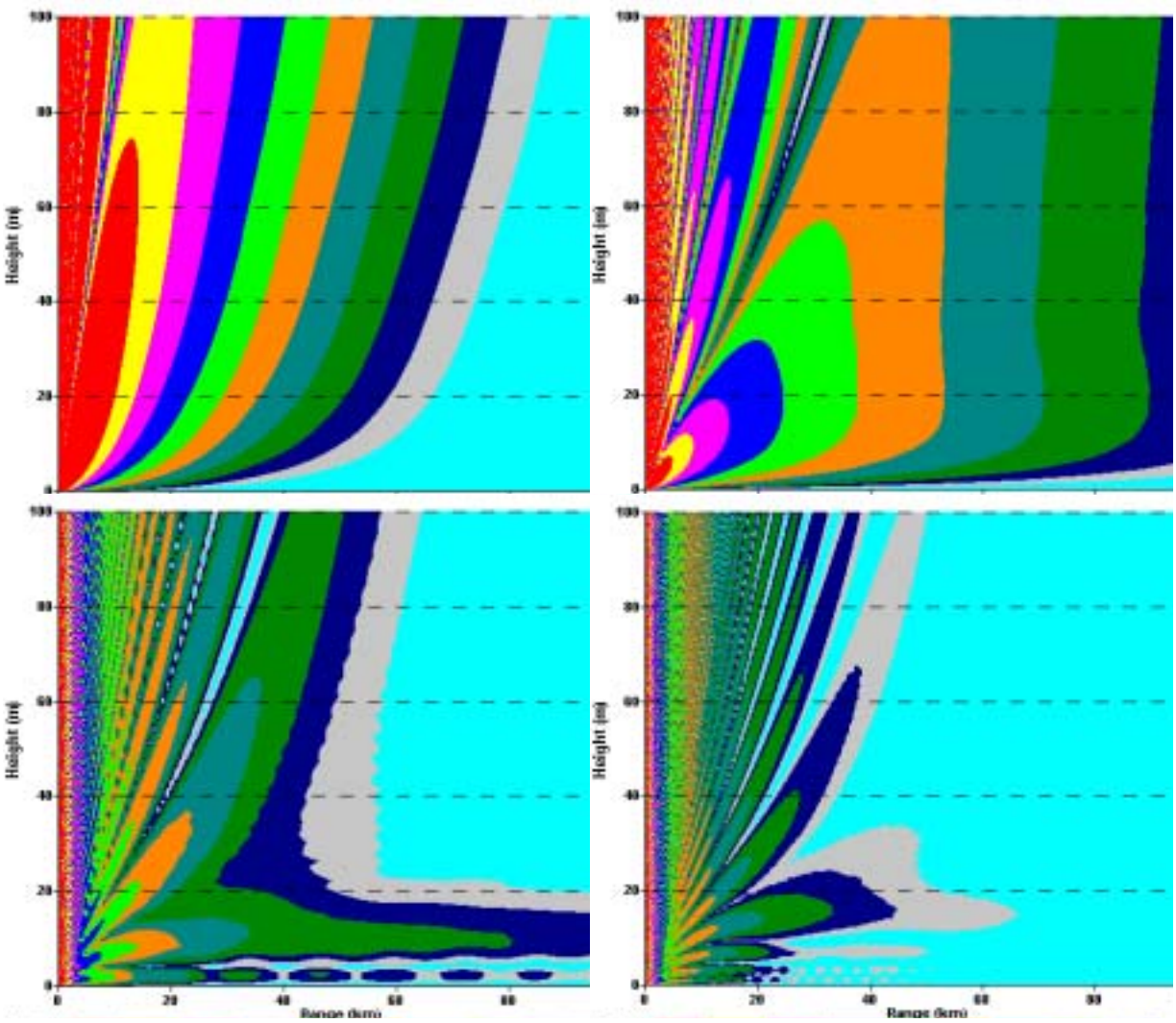

Figure 3. Propagation loss (dB) versus distance (km) for an environment with an evaporation duct height of 20 m and an antenna height of 10 m. Top left: L-Band (1 GHz); Top Right: S-Band (3 GHz); Bottom Left: X-Band (10 GHz); Bottom Right: Ku-Band (18 GHz). The color scheme is the same for all four panels. Red: <110 dB; Yellow: 110-115 dB; Magenta: 115-120 dB; Blue: 120-125 dB; Green: 125-130 dB, etc.

II. DATA COLLECTION

The Roughness and Evaporation Duct (RED) experiment was designed in response to the recognition that propagation models seem to underestimate loss at high frequencies over water surfaces in the presence of high winds. This could be due to problems with current ABL theories, which include the bulk method, or surface scattering in the presence of high winds and rough surfaces, but the exact cause has not yet been determined. The purpose of the combined METOC data and propagation collection was to relate the effect of both the ABL and ocean surface roughness to high frequency electromagnetic propagation. To that end, ABL and ocean surface data and propagation data, were collected from August to September 2001 off the windward coast of Oahu, Hawaii during the RED experiment. The Oahu location was chosen because the warm sea surface in the trade wind region produces strong evaporation ducts and rough surfaces.

A. NAVAL POSTGRADUATE SCHOOL (NPS) 'FLUX' BUOY

The NPS 'Flux' buoy was located roughly 5 km west of R/P FLIP at 21° 40.623'N, 157° 53.210'W (Fig 4 & 5). The buoy collected atmospheric surface layer and ocean surface data continuously at one-second intervals from August 22, 2001 0240Z until September 18, 2001 1554Z. The NPS buoy collected pressure data at 0.39 meters above the sea surface, wind speed and wind direction data at 4.15 meters, and air temperature and relative humidity data at 4.08 meters above the surface. The buoy collected sea surface temperature measurements with an infrared radiometer mounted 3 meters above the sea surface. The environmental measurements were averaged to one hour bins centered at the hour. Unfortunately, the data collected at the DREV buoy was not available. The buoy-measured METOC time series represent those that could be made available in real time on a surface combatant. In fact, sensors and collection procedures for the buoy were selected and tested within the R&D portion of the acquisition program the led to the SMOOS(R) systems.

B. COAMPS

The COAMPS model runs were performed by the National Research Laboratory (NRL) Washington DC for the purpose of an aerosol trajectory study that was part of the RED experiment. NRL was kind enough to allow us to use their model results for this study. The COAMPS models were run using three nested configurations having horizontal grid spacings of 27, 9, and 3 km (Fig 6). The models were run at 00Z and 12Z, and produced hourly forecasts from the analysis time through the 12-hour forecast. The model grid point locations for each resolution were plotted with the locations of the NPS 'Flux' buoy, R/P FLIP, the receiving station, the propagation path, and the Oahu coastline. The best representative grid points were chosen from this plot. The lower resolution 27 km grid yielded two offshore grid points, the 9 km grid bracketed the propagation path with five grid points, and the highest resolution 3 km grid yielded seven grid points along the propagation path (Fig 4). The land-sea field was checked to ensure that all of the chosen grid points were modeled over water.

For the bulk method, the only environmental input parameters needed are the sea surface temperature, and air temperature, wind speed, relative humidity, and pressure at a known height. The lowest sigma level of the COAMPS model runs (which has a height of 10 m) was used because the model produces U and V wind components, potential temperature, water vapor, and pressure fields at the sigma levels hourly. The sea surface temperature field in COAMPS is constant for each model run. A small program was written to pull the values of the selected fields at the chosen grid points for each hourly time from the flat files of each domain. From these data the wind speed, air temperature, and relative humidity were calculated. The grid points for each model resolution were simply averaged for each time step.

The relationship between the forecast level and the surface in the version of COAMPS used for this study was based on the Louis (1979) surface layer parameterization scheme (Hodur 1996). In this scheme polynomial functions of the bulk Richardson number, $Ri_B = zg\Delta\theta/(U^2\theta)$, are used to directly compute the surface fluxes. These and the surface boundary conditions establish mean values in the lower levels. The COAMPS option for the surface layer parameterization based on the TOGA-COARE

scheme (Fairall et al. 1996) was not available but is important to note because it forms the basis of the NPS bulk model, which was used to calculate the profiles that were then applied to APM. The TOGA-COARE scheme differs from the scheme used in older versions of COAMPS by:

Different functional forms for z_{0t} and z_{0q}

Use of similarity theory directly

Polynomial approximation for stability function on the unstable side

C. S-, X- AND KU-BAND PROPAGATION DATA

Onboard the R/P FLIP (Fig 7), positioned at 21° 41.082'N, 157° 50.433'W, a "High antenna" at 12.62 m and a "Low antenna" at 4.88m (nominal heights above the sea surface) transmitted radio waves at three frequencies: S-Band (2.975 GHz), X-Band (9.7 GHz) and Ku-Band (17.7 GHz). Over the course of the experiment the displacement of the R/P FLIP changed slightly (due to fuel and stores consumption, etc.). The resulting changes in antenna height were recorded and accounted for.

The receiving antenna positioned at 21° 27.495'N, 157° 45.999'W, was on shore 25.77 km away, at a nominal height above sea level of 4.73 meters. Tidal fluctuations, which changed the effective height of the receiver from the sea surface (a range of 4.2m to 5.1m), were recorded and accounted for. Propagation loss was measured on a five-minute cyclic basis for each of the six-frequency/antenna height combinations (for example the "High S-band" combination would occur from 00-05 and 30-35 minutes past every hour). The propagation data were averaged over the five-minute collection periods, resulting in one averaged value for each frequency/antenna height combination every thirty minutes. The prop losses from the half hour before the hour, and the half hour after the hour, were averaged to give a prop loss at the hour (for comparison with the two prop loss prediction methods).

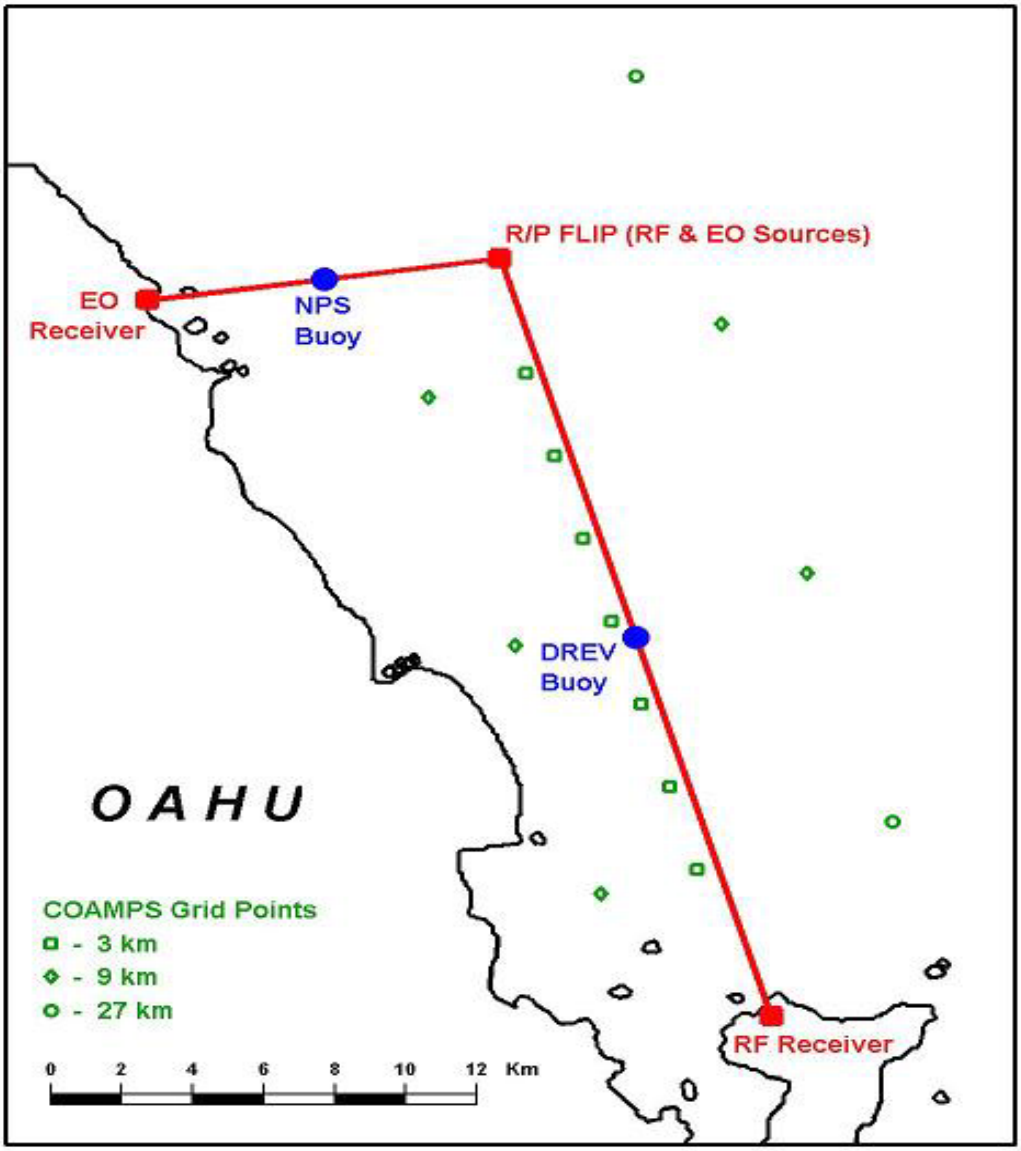

Figure 4. Map of the RED layout showing the location of the NPS Flux Buoy, RP FLIP, RF Receiver, RF Transmission Path, and the COAMPS Grid Points. The green circles are the two 27km grid points, the green diamonds are the five 9km grid points, and the green squares are the seven 3km grid points.

Figure 5. The NPS Flux Buoy.

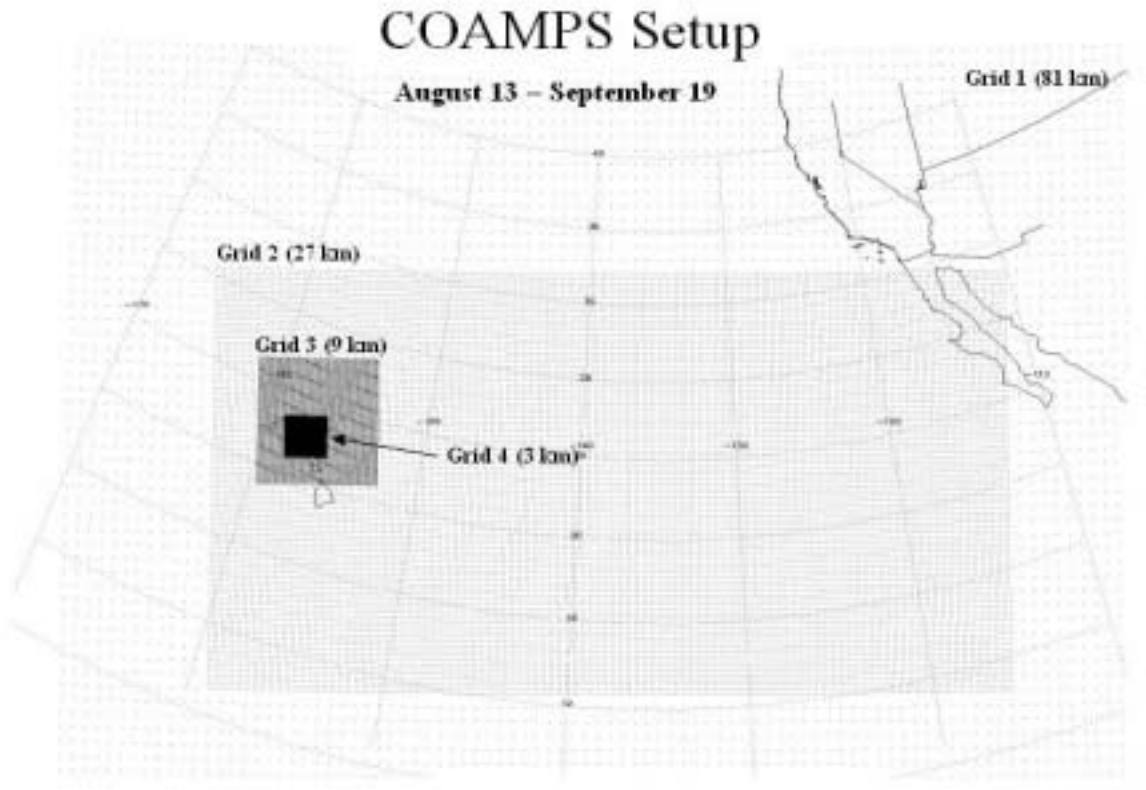

Figure 6. Map showing the COAMPS grid domains of the 27, 9, and 3 km resolution models.

Figure 7. R/P FLIP.

THIS PAGE INTENTIONALLY LEFT BLANK

III. DATA ANALYSIS

A. NPS FLUX BUOY AND COAMPS METOC PARAMETERS

Unfortunately the COAMPS modeled METOC data could not be directly compared to the buoy observations because the COAMPS parameters were provided at 10m and the buoy data was measured at heights of 0.39m, 4.08m, and 4.15m, as stated earlier. In order to compare 'apples to apples', the buoy-measured data was input into the NPS bulk model, which created ABL profiles. The 10m METOC values from these profiles were used for comparison with the 10m COAMPS values. Figures 8, 9, and 10 show the time series of the relative humidity (RH) in %, air temperature (Tair) in °C, sea surface temperature (SST) in °C, and wind speed (WS) in m/s. The observations measured at the NPS Flux Buoy are in red, and the COAMPS forecasts are in blue. Figures 8, 9, and 10 compare the buoy observations to the 27, 9, and 3 km resolution COAMPS forecast output, respectively.

Overall the buoy-observed RH, SST, Tair, and WS don't vary much from the mean conditions, but the data does show quite a bit of small-scale variability over very short time periods. With the exception of a few outliers, the RH is 75% +/- 5%; the SST is 26-27°C; the Tair is 25-26°C, and the WS is 6 m/s +/- 2 m/s over the entire 18-day period. There are only a few significant deviations from the mean conditions. A short period (~4hr) of high RH and low Tair occurs on day 242, with a similar event on day 252. The winds increased to greater than 8 m/s for ~48hrs centered around 12Z on day 243. Wind speeds died down to less than 4 m/s for ~5hrs late on day 257. Lastly, the RH on day 258 peaks at ~90%. Other than the above anomalies, the weather was surprisingly consistent.

The diurnal signal is fairly weak but evident in the Tair and SST data. With 00Z occurring at 2:00 pm local time the maximum temperatures are found just after 00Z and are well within 2°C of the minimum temperatures. The WS and RH also show a diurnal signal with wind minimums around 00Z, wind maxima around 09Z, and the RH diurnal signal is inversely related to the Tair. In August and September, Hawaii's tropical marine location exhibits a relatively small magnitude diurnal signal.

The buoy data were averaged from measurements at 1-second intervals from 30 minutes before the hour to 30 minutes after. Most of this variability could be removed by averaging over a 3-hour period, and would have created much smoother time series plots, but would not depict the true nature of the atmosphere. The noisy nature of the METOC parameters does present a problem when trying to interpret the statistical results and will be discussed in greater detail later in the thesis. For the purposes of this discussion, all buoy observations were assumed to be accurate although they possess small errors.

The most obvious difference between the buoy observations and the COAMPS data is that COAMPS uses a fixed SST for each 12hr model run. Although COAMPS is a 'coupled' model, it doesn't forecast changes in SST but rather uses a SST field from NOGAPS 1^{o} gridded analysis as an input only. In its present operational configuration, SST does influence the atmosphere above it, but the atmosphere does not influence the SST. The SST input is updated every model run to account for changes, but no sea surface heating or cooling is accounted for during the model run. The COAMPS SST was consistently greater than the measured SST, but was almost always within 1°C. It is also important to remember the position of the NPS flux buoy, which was located 5 km West of the RP FLIP at the North end of the propagation path (Fig 4).

Overall COAMPS did a very respectable job of modeling and predicting the atmosphere. The COAMPS Tair and WS were especially close to observed values. The increased winds around day 243 were well depicted, and the slacking of the wind late on day 257 was especially well captured. The Tair predictions were usually within 1°C of the observed. The RH plot is the most variable and noisy of the METOC parameters both for the observed and the COAMPS modeled data and therefore, it is difficult to determine if COAMPS did a good job of predicting the RH. The METOC parameter trends, that occurred over time periods of greater than 4 or 5 hours were evident in the COAMPS model output, which is impressive. However, COAMPS did not capture the short-term variations, like the cold Tair events on day 242 and 252. It appears that these were “local” mesoscale events that would be difficult to initialize in COAMPS. Additionally, COAMPS predicted a few events that were not observed by the buoy. The most obvious error is a predicted slacking of the winds on day 247, which did not occur.

In Figures 8, 9, & 10 the COAMPS 00Z and 12Z analysis values are depicted by a black square. Surprisingly, many of the outlying COAMPS predictions are the analyses values. This is most obvious in the Tair plots. There are actually two values for each 00Z and 12Z time because the earlier 12 hr forecast value and the later analysis have the same valid time. Both were plotted, but the black square was used to show which one was the analysis. It is believed that the analyses errors are at least partially due to the inclusion of erroneous observations, which negatively impact the models through the multi variant optimal interpolation (MVOI) process. These observations force the model fields out of dynamic balance, which is resolved after a few time steps.

When comparing the forecast skill of the 27 km COAMPS against the 9km and 3km resolution models, it is important to remember the location and number of grid points which were used in this study (Fig 4). The SST field for all of the resolutions is exactly the same. The 27 km COAMPS, which only used two offshore grid points, was less accurate for the Tair and RH in the period from day 247 to 250, but overall did reasonably well. The 27 km WS is too high for almost all of the period from day 241 to 246, but shows the proper overall trend. The 9 km resolution model output for the Tair and WS is very good, with the exception of a few of the analysis values. There are three instances where the wind speed is significantly under-predicted, the worst being on day 247. The 9 km COAMPS RH values and observed RH are very noisy and therefore differ quite a bit. The 3km COAMPS Tair plot is impressively similar to the buoy observed data with the exception of the two short-term cold air events. The 3 km WS plot is very similar to the 9 km values except that most of the deviations from the mean values are just slightly more exaggerated in the 3 km plot. The 3 km RH is slightly closer to the observed than the 9 km and is most likely related to the improved Tair values. In my opinion the differences between the 3 and 9 km model outputs would not justify the cost in computer run time and memory needed to run the higher resolution 3 km COAMPS.

B. EVAPORATIVE DUCT HEIGHT PREDICTION

In order to predict the EDH, all of the METOC parameters (and their heights) from the NPS buoy observations and the three different resolution COAMPS models were input into the NPS bulk method evaporation duct model. The NPS model created ABL profiles from this input and determined the height of the minimum M value from each profile; the EDH. The top panel of Figures 11, 12, & 13 show the resulting buoy data derived EDH time series vs. the COAMPS derived EDH of the 27 km, 9 km, and 3km resolution models, respectively. As in the prior plots, the buoy observation derived values are in red, the COAMPS forecasts are in blue, and the COAMPS analyses are highlighted with black squares.

Not surprisingly, the EDH time series plots are as noisy as the METOC parameters they are based upon. The buoy derived EDH shows a normal range of 10 to 13 m with significant short-term small-scale variability. There is a period of elevated EDH (13-15 m) from day 242 through 245 corresponding to the period of increased WS. There are also 'spikes' of lower EDH (well below 10m) which correspond to periods of increased RH (greater than 80%). In over-simplified terms, increases in WS increase the turbulent mixing of the ABL and increase the height of the evaporative duct. Also, increases in RH reduce the normal RH gradient that is the dominating force that causes the EM refraction, which lowers the EDH.

When comparing the COAMPS forecast derived EDH to the buoy derived EDH, it's important to point out that there was no direct measurement of the EDH to compare them both too, but that they are both just products of the METOC parameters that were input into the NPS bulk model. All of the apparent errors in the EDH are the direct result of differences in the METOC values. Overall the COAMPS EDHs are similar to the buoy EDH. Obviously, the error prone analyses time COAMPS data leads to poor agreement between the flux buoy- and COAMPS-derived EDH values at those times. Also, the incorrect wind speeds of day 247 result in very low EDHs. As discussed in the last section, the 27 km COAMPS output is not as good as the 9 or 3 km resolution data, but all are fairly close to the buoy-based EDH values. Overall trends are well depicted in

the COAMPS output, but the short-term small-scale variations are not. The noisy nature of the METOC inputs creates noisy EDH plots.

In order to more precisely evaluate the COAMPS EDH output against the buoy-derived EDH values, the root mean squared (RMS) and mean difference of the COAMPS values from the buoy-derived values (in meters) were plotted against time (Fig 14). The time axis is displayed in both forecast time and the corresponding local time. This allows diurnal effects and forecast time effects to be analyzed. Due to the valid time overlap of the previous 12-hour forecast and the next model run's analysis, there are two plots for 1400 and 0200 local. The 27 km resolution COAMPS values are in blue, the 9 km in red, and the 3 km COAMPS in green.

All of the RMS differences were between 2.5 and 1.4 m with the exception of the analysis times. The 27 km and 9 km COAMPS 00Z analyses and 3km 12Z analyses had RMS differences of greater than 2.5 m. It is surprising to see that there are times when the 27 km model has the lowest RMS, times when the 3 km or 9 km models show the best RMS, and conversely each of the resolutions have times when they have the highest RMS. On average the 27 km resolution model differed from the buoy-derived EDH the most, the 9 km model performed the best during the late night and early mornings, and the 3 km COAMPS handled the warmest part of the day best.

The mean difference plot is much easier to decipher. None of the hourly time bins had a mean difference of more than 2 m. The 27 km COAMPS tended to over-predict the EDH especially in the first three hours of each run and also at the end of the 00Z run. The mean differences of the 3 and 9 km resolution COAMPS are very similar and are always less than the 27 km model. Both the 3 and 9 km models under predict the EDH during the late afternoon (1700-1900). The most interesting results are during the late morning when the 27 km and 3 km models have very similar results and are near 0, but the 9 km resolution model continues to under-predict the EHD by ~1 m. For the most part, the mean differences between the model and buoy EDH are within 1 m, which is quite good, but there is no obvious correlation between the RMS and mean difference.

C. PROPAGATION LOSS

The ABL profiles that were created by the NPS bulk method evaporation duct model from the buoy observations and the COAMPS modeled METOC parameters were input into APM, which is the propagation prediction model included in AREPS. From this input, APM predicted propagation loss values across the ~26 km propagation path for the two transmitter heights. The propagation loss between RP FLIP and the receiving station was also measured directly. Due to equipment failures there is a gap in the prop loss measured data for parts of days 252, 253, 256, 257, and 258. Propagation loss measurements and predictions were made for S, X, and Ku band radar wavelengths but the results were so similar that only the S band results will be discussed (for the sake of conciseness).

The middle and lower panels of Figures 11, 12, and 13 are time series plots of propagation (prop) loss measured between RP FLIP and the shore based receiver (in green), derived from the buoy observations (in red), and predicted by the COAMPS models (in blue). The middle panel shows the prop loss for the upper transmitter (12.6 m) and the lower panel shows the lower transmitter values (4.9 m). The lower transmitter was always within the evaporative duct, but the upper transmitter was above the EDH at times. The onshore receiver (at 4.7 m) was always within the evaporative duct. Figure 11 shows the 27 km resolution COAMPS, Figure 12 the 9 km, and Figure 13 depicts the 3 km resolution model-derived propagation losses. The measured prop losses (green) and buoy data derived prop losses (red) are the same on Figures 11, 12, & 13, which only differ in COAMPS model resolution.

The measured prop loss for the upper transmitter varies from a low of 137 to a high of 151 dB with a mean of 144 dB. The measured prop loss for the lower transmitter varied from 144 to 154 dB with a mean of 150 dB and one large spike of up to 159 dB on day 257. The measured prop loss data contains a great deal of variability and is marked by a few peaks of lower prop loss and many spikes of high prop loss which last for 5 or 6 hours, on average. The spikes of greater prop loss are more prevalent in the upper transmitter prop loss plot. For the sake of this discussion, the measured prop loss values are assumed to be without error. The buoy observation derived prop losses are very

similar in range to the measured prop losses, although on average they under-predict the prop loss by a dB or two and do not capture many of the high prop loss spikes that show up in the measured prop loss data. For the most part the buoy-derived values are within 2 dB of the measured prop loss.

The performance of the COAMPS-derived prop loss predictions is very similar to the buoy data-derived values. Overall the COAMPS derived prop losses are within a few dB of those measured. The 27 km resolution COAMPS produces the worst results with periods of under-prediction on days 244, 246, and 254 and over-predictions on days 247, and 249. It is easy to see the direct correlation between elevated EDH and low prop losses in the model-derived plots. Wherever the model METOC parameters lead to an over-prediction of the EDH, there is a corresponding under-prediction of the prop loss values and vice versa. The most obvious of these is the under-predicted EDH of the 3 and 9 km COAMPS on day 247 (which was due to an under-prediction of the wind speeds) that results in an over-prediction of the prop loss values. Overall the 3 and 9 km COAMPS data yield very respectable prop loss predictions (with the exception of the afore mentioned analyses errors) that are usually within 2 dB of the measured values, and are often closer than the buoy-derived values. However, like the buoy derived prop losses, the COAMPS forecast derived values do not capture the short-term high prop loss spikes that are a dominant feature of the measured prop loss plots.

In order to take a more objective look at the performance of the buoy- and COAMPS-derived prop losses, the root mean squared (RMS) and mean difference of the COAMPS and buoy-derived values from the measured prop loss values (in dB) were plotted against time. Figure 15 shows the lower transmitter prop loss and Figure 16 is for the upper. The time axis is displayed in both forecast time and the corresponding local time. This allows forecast time effects and diurnal effects to be analyzed. Due to the valid time overlap of the previous 12-hour forecast and the next model run's analysis, there are two plots for 1400 and 0200 local. The 27 km resolution COAMPS values are in blue x's, the 9 km are red squares, the 3 km COAMPS are green circles, and the buoy observation-derived values are black triangles.

The RMS buoy values range from 1 to just over 3 dB with periods of low RMS in the evenings (1800-2100 local) and higher RMS values in the late mornings (0800-1100 local). The mean difference plot shows that the buoy based prop losses are usually under-predicted but are always within 3 dB. With an average RMS of ~2 dB and a mean error of ~-1.5 dB, the buoy observation-derived prop loss predictions are very good.

With the exception of the analysis times, the COAMPS based RMS differences are all less than 4.5 dB and average ~3 dB. The COAMPS mean difference values follow the trend of the buoy-based values very closely. The 27 km resolution model tends to under-predict the prop loss much like the buoy-derived values, while the 3 and 9 km COAMPS prop loss mean differences are always within 2 dB and are pretty consistently ~1 dB higher than the buoy and 27 km resolution values.

Figures 15 and 16 contain an interesting feature, evident in the evenings between 1800 and 2100 local. During this time the buoy-based prop loss values are very close to the measured values, and the COAMPS forecasts are particularly poor. Also, there is an obvious increase in the COAMPS RMS errors and the mean differences indicate over-predictions. If the data from this time period were excluded from the prop loss plots it would be easy to conclude that the buoy-based prop losses are consistently under-predicted by ~1.5 dB, have little variability, and could likely be corrected for by 'tuning' the NPS bulk method evaporative duct model or the APM. Along the same lines, you could conclude that the COAMPS-based prop losses had less of an under-prediction bias but more variability than the buoy-based values, and that the higher resolution 3 and 9 km models out-perform the 27 km COAMPS. However, the inclusion of the evening values contradicts all of the above conclusions. At this time it is unknown what is affecting the prop losses in the evenings, but may be related to rain showers that affect the RH gradient, or a slacking of the winds, which decreases the roughness of the sea surface and prop loss due to scattering.

Figures 17 through 22 are scatter plots of the COAMPS (blue x's) and buoy (red circles) derived vs. the measured prop losses. Each figure has 6 panels that are plots of different forecast times (anal, 2, 4, 6, 9, and 12 hour forecasts). The first three figures (17-19) are for the lower transmitter height and the second three are the upper (20-22).

The two sets of three figures are for the 27, 9, and 3 km resolution COAMPS data, respectively. Points falling on the thick dashed line are equal to the measured values, and are bounded at +/- 5 dB by a thin dotted line. Also included are the correlation, RMS and mean differences for each panel's data. These plots were created to see if there is a correlation between model forecast time and accuracy.

The buoy-based prop losses fall close to the measured values in a tight grouping resulting in small RMS errors, and are fairly consistently under-forecast. The upper transmitter plots show greater variability as would be expected considering that the upper transmitter was both above and below the EDH. The COAMPS-derived prop losses show a greater variability than the buoy-based values, but show no definite bias. These plots show the reduced accuracy of the model analysis output compared to the other forecast times. There is no apparent loss in forecast accuracy with increased forecast time over the short 12-hour forecast period. Also, as demonstrated in other figures the 3 and 9 km resolution COAMPS models out perform the 27 km. Overall there are very few data points outside of the +/- 5 dB bounds.

D. POSSIBLE DATA ERROR SOURCES

The RP FLIP was used as the base for the radar transmitters and due to its design it provides a very stable floating platform. However there were also some problems caused by its unique shape. The extreme length of its hull allows it to maintain a constant height above the sea surface regardless of the waves and swell. Due to the RP FLIP's mooring, it twisted on its vertical axis, which changed the direction that the radar transmitters were pointing in. Figure 23 shows the deviation in FLIP's heading. Normal deviations are between 0 and +/- 12°, with extreme deviations as large as ~25°. These deviations in the transmitter headings should erroneously increase the measured prop loss values, and are a possible source of the greater than predicted prop loss values discussed earlier. As stated earlier all observed METOC observations were assumed to be perfectly accurate, although measurement and equipment calibration errors may be the source of the apparent NPS flux buoy based prop loss prediction's ~1mB bias.

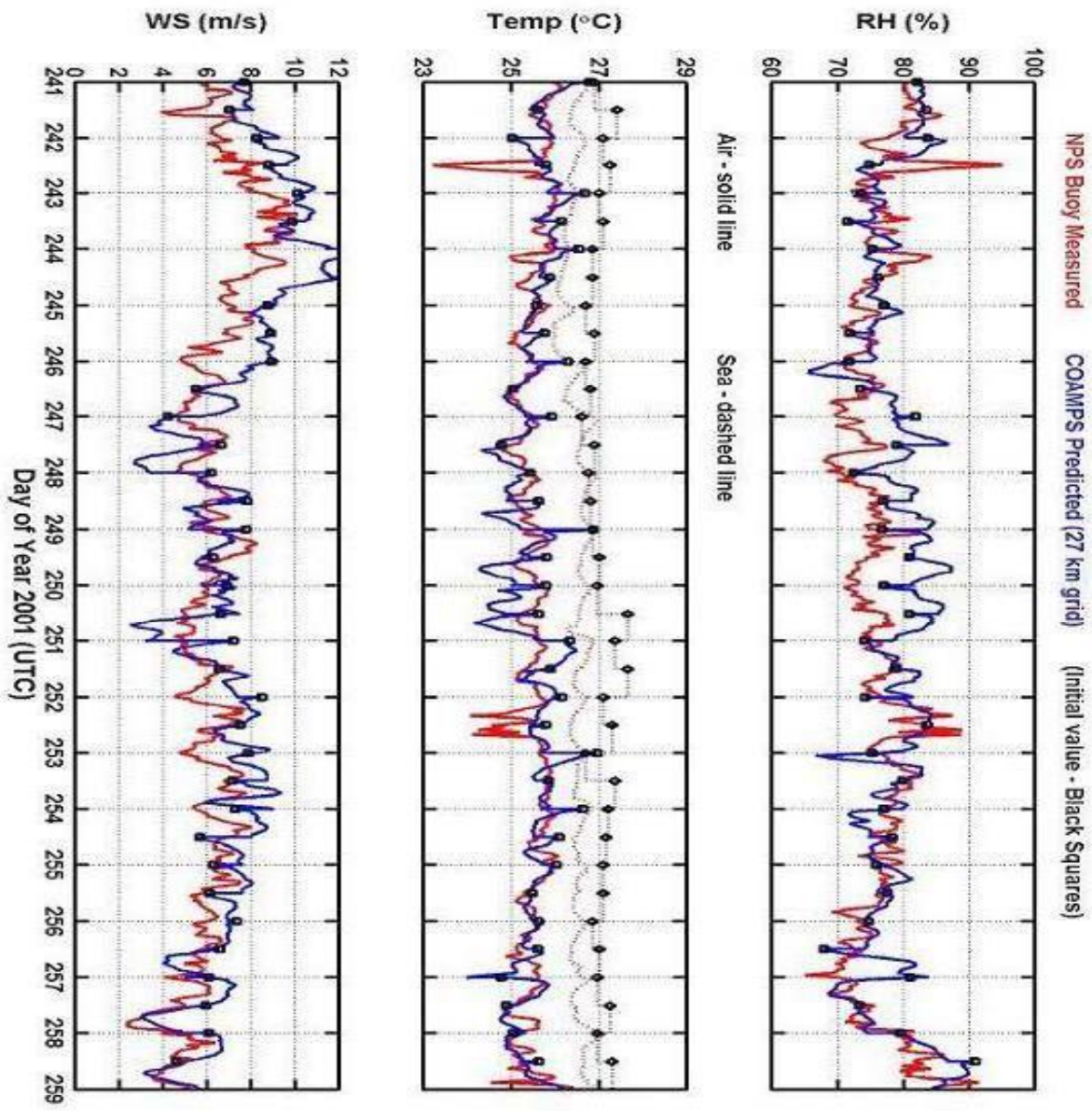

Figure 8. Time series of RH (%), SST (°C), Tair (°C), and WS (m) measured at the NPS Flux Buoy (red) and forecast by the 27 km resolution COAMPS model (blue). Black squares indicate model analysis values.

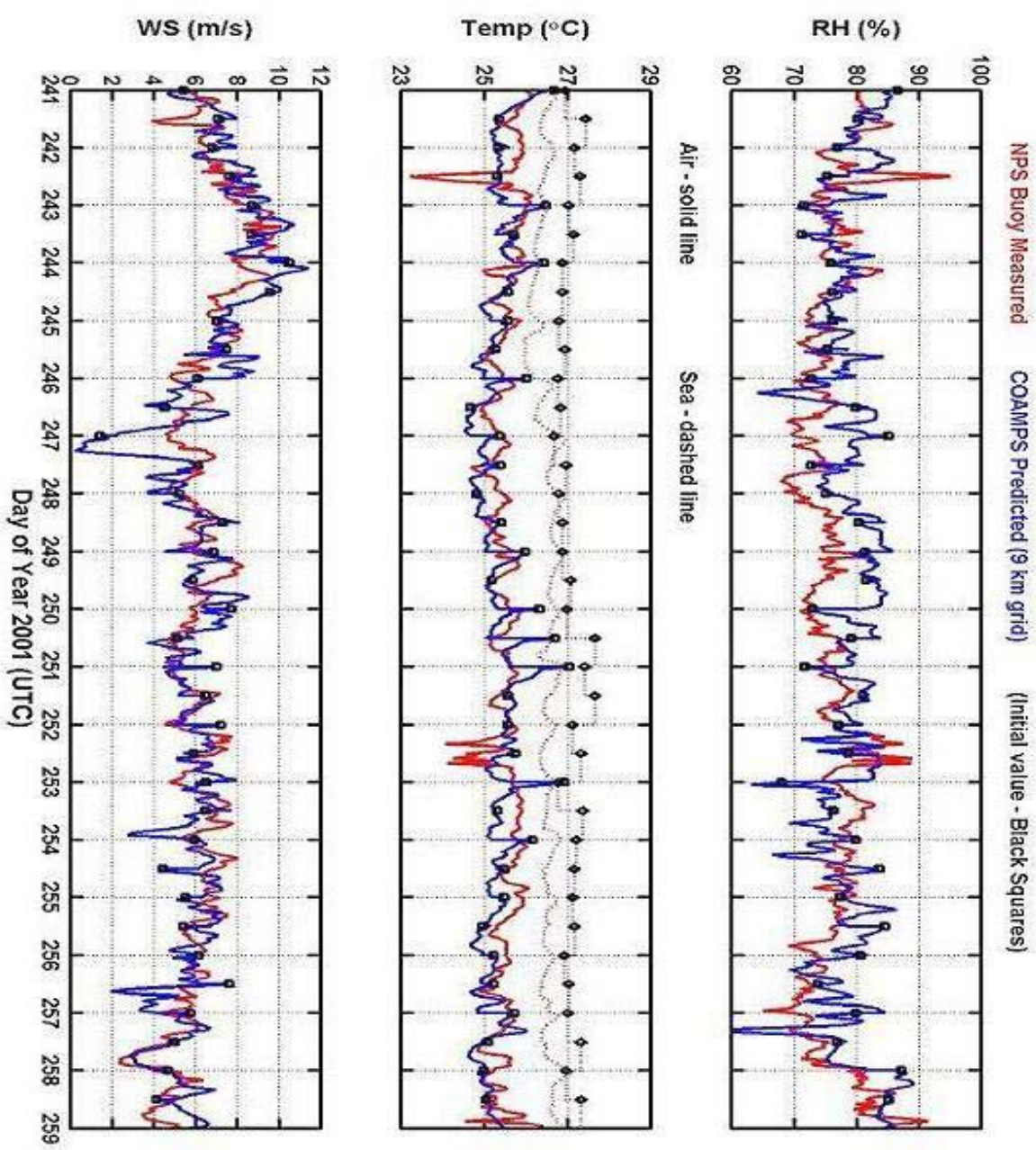

Figure 9. Same as Fig 8 except 9 km resolution COAMPS data.

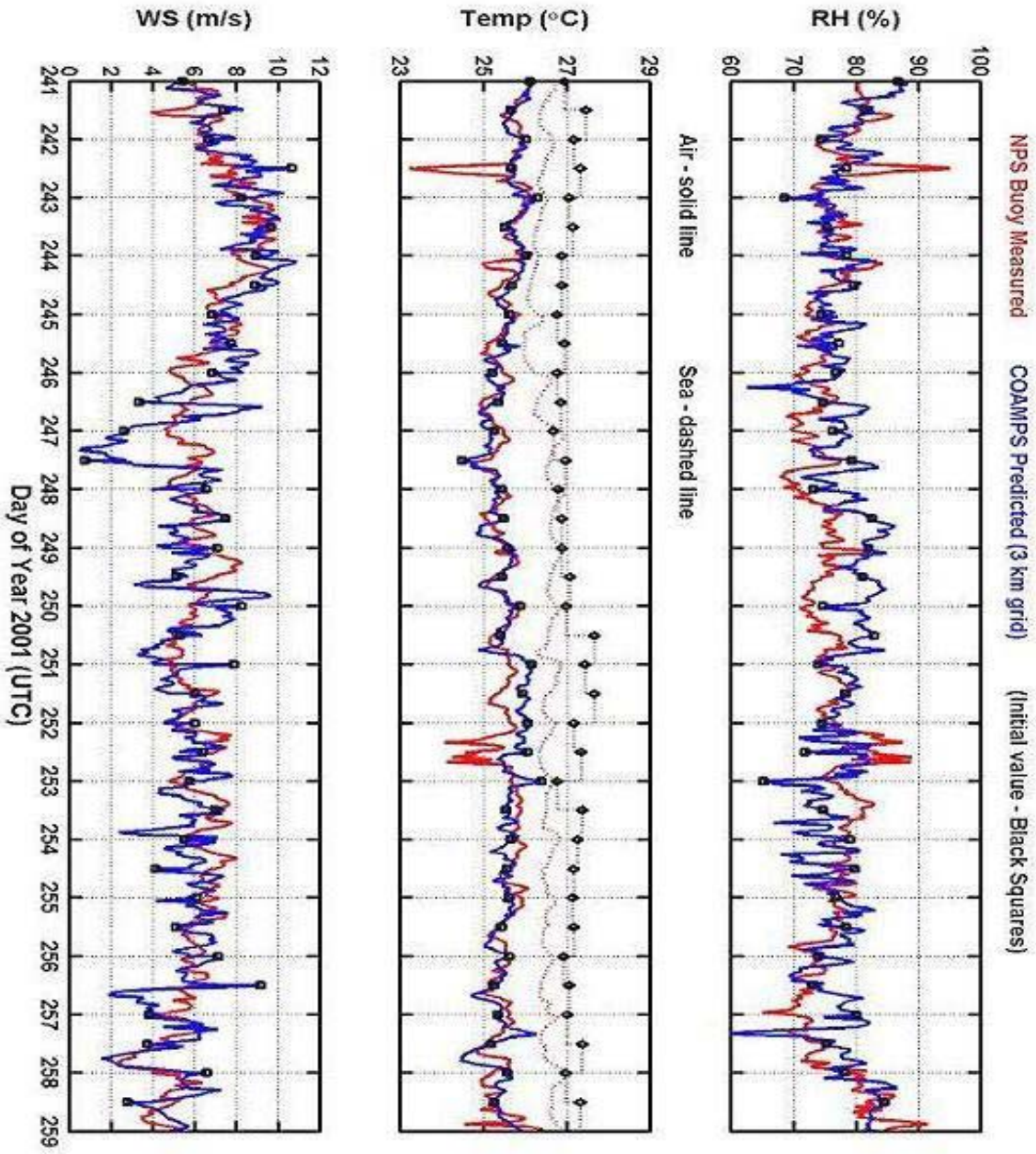

Figure 10. Same as Fig 8 except 3 km resolution COAMPS data.

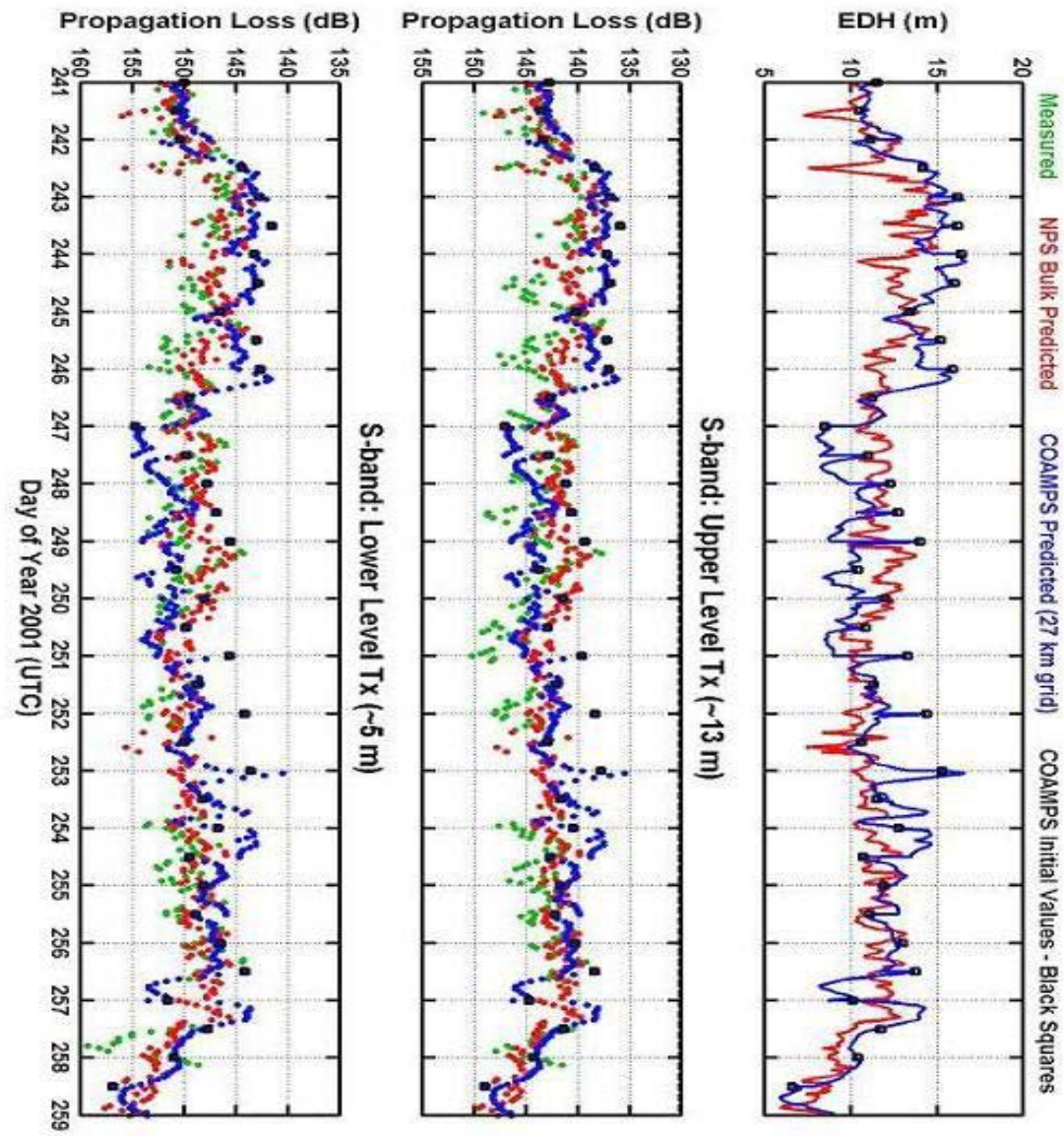

Figure 11. Time series of NPS bulk evaporation duct model predicted EDH (m), and Upper and Lower level transmitter Prop Loss (dB), based on buoy measured METOC data (red) and 27 km COAMPS forecast data (blue). Green dots are measured Prop Loss values. Black squares indicate model analysis based values.

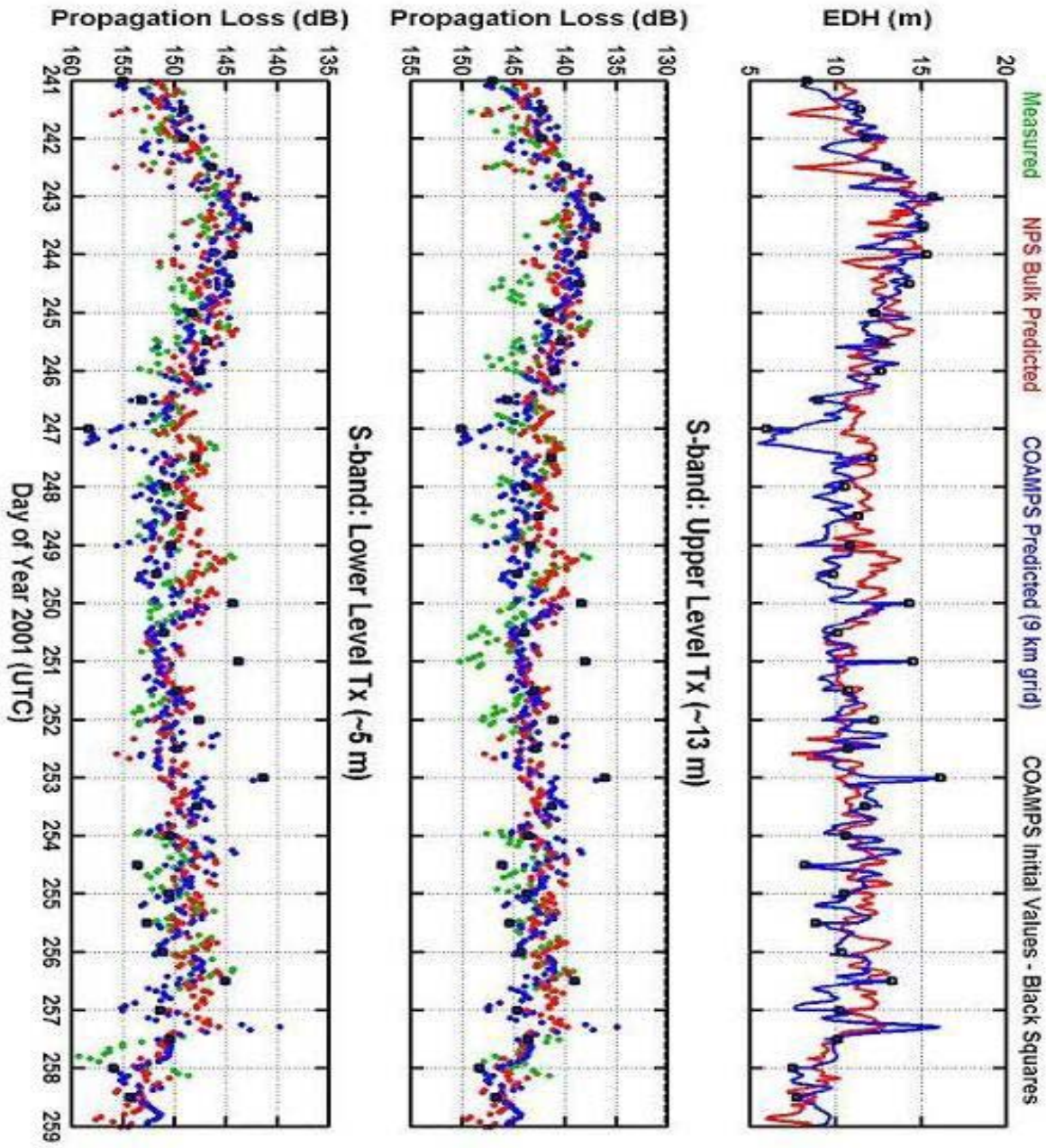

Figure 12. Same as Fig 11 except 9 km resolution COAMPS based data.

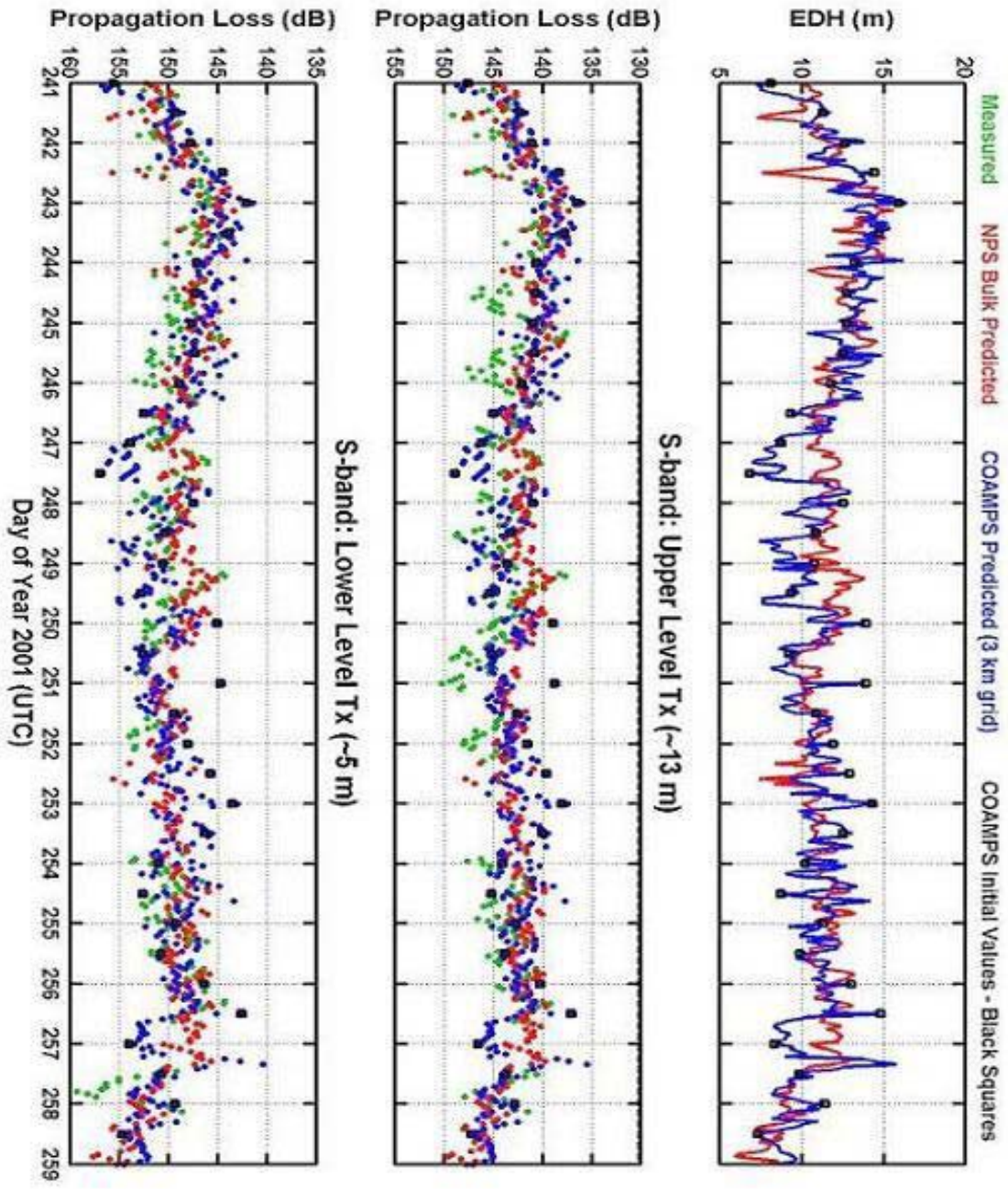

Figure 13. Same as Fig 11 except 3 km resolution COAMPS based data.

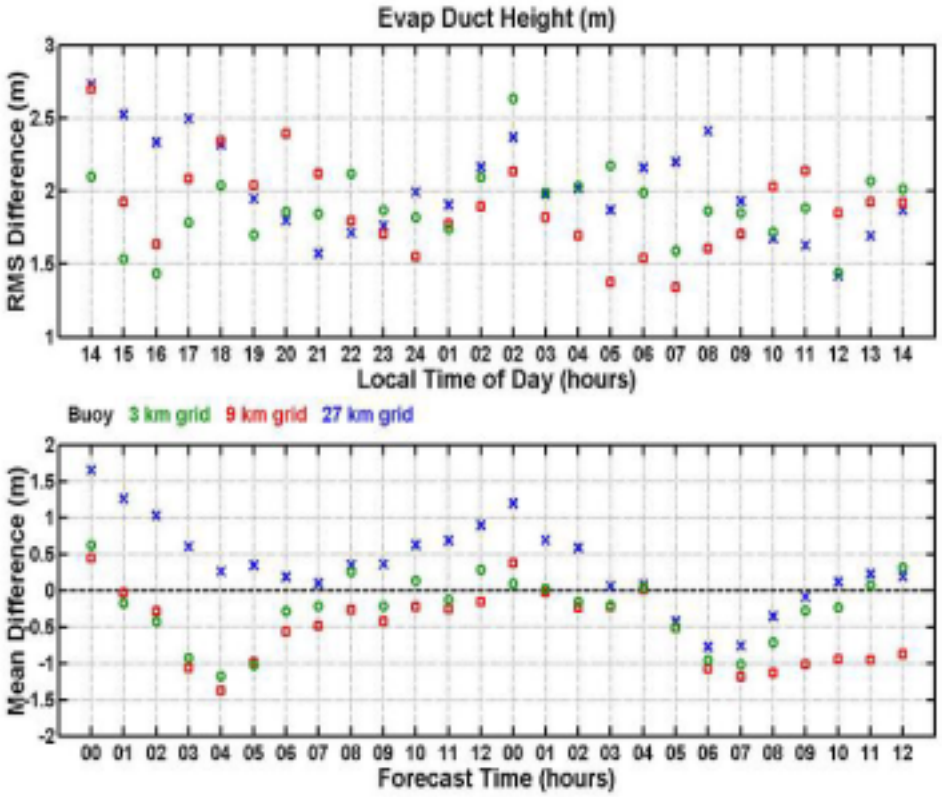

Figure 14. RMS (m) and Mean Difference (m) between the buoy measurement based EDH predictions and the COAMPS data based EDH predictions for each hour. Blue X's are 27 km resolution COAMPS data, red squares are 9 km resolution, and green circles are 3 km COMAPS resolution values. The time axis is in both forecast time and local time.

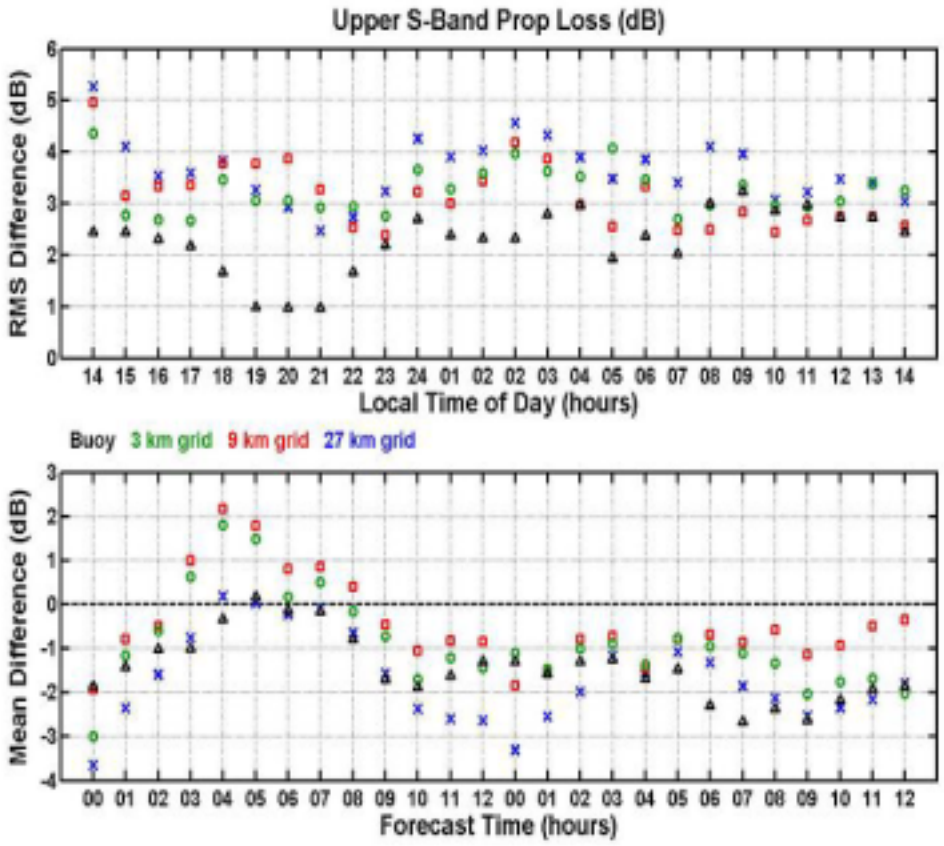

Figure 15. Upper level transmitter Propagation Loss RMS (dB) and Mean Difference (dB) between the in situ measured Prop Loss and the buoy measurement based Prop Loss predictions and COAMPS data based Prop Loss predictions for each hour. Black triangles are buoy measurement based values, blue X's are 27 km resolution COAMPS data, red squares are 9 km resolution, and green circles are 3 km COMAPS resolution values. The time axis is in both forecast time and local time.

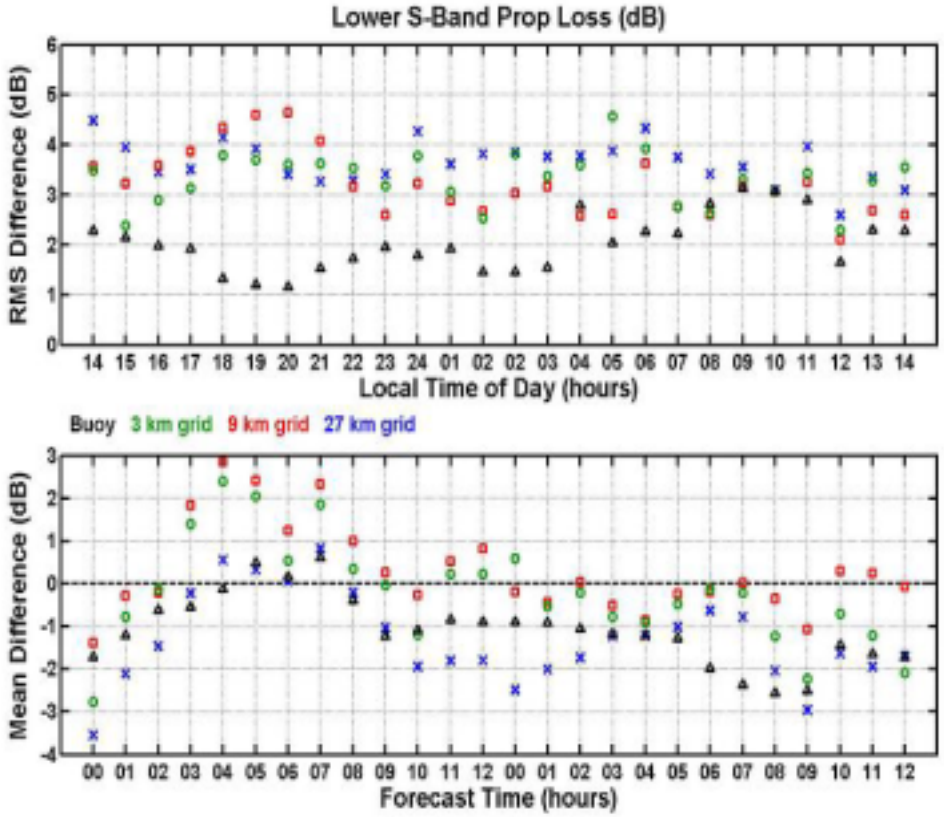

Figure 16. Same as Fig 15 except Lower level transmitter Propagation Loss data.

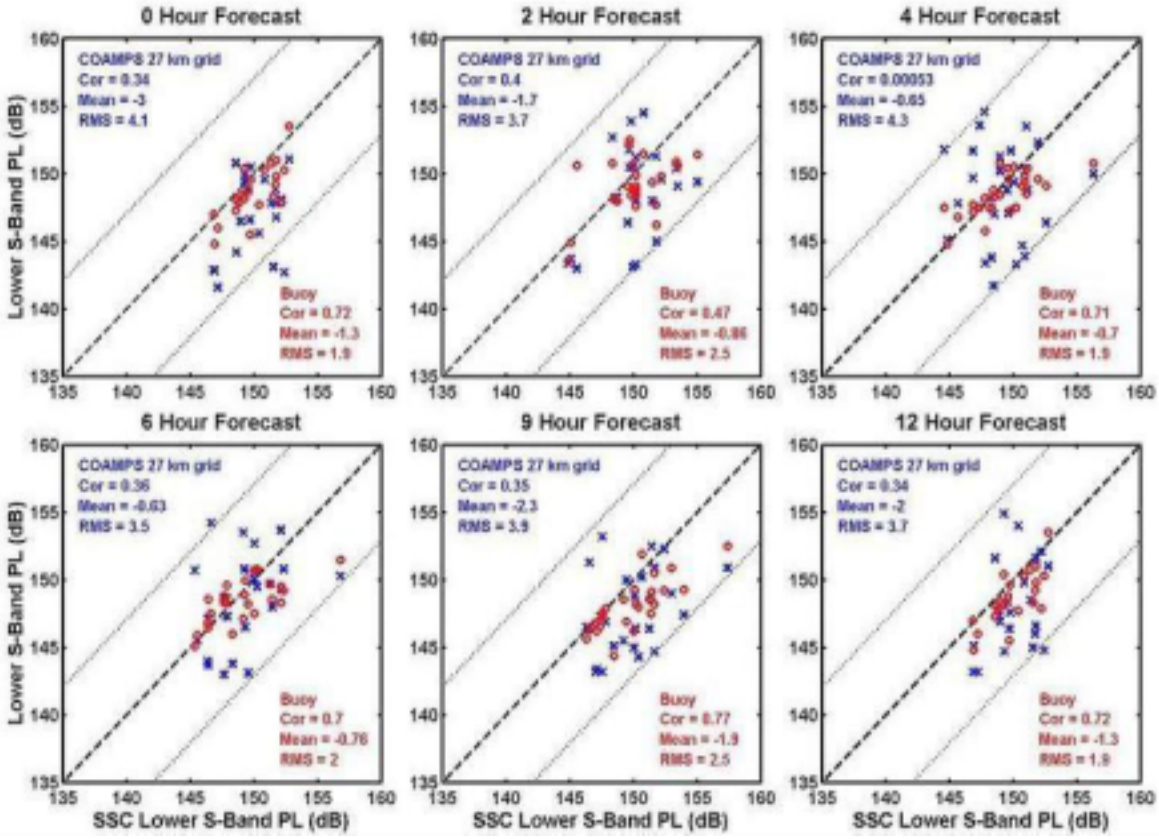

Figure 17. Scatter Plot of the Analysis, and 2, 4, 6, 9, and 12 hour forecast time Lower transmitter Propagation Loss prediction values. X-axis is measured Prop Loss, Y-axis is predicted Prop Loss. Blue X's are 27 km resolution COAMPS based data; Red circles are Buoy measurement based values.

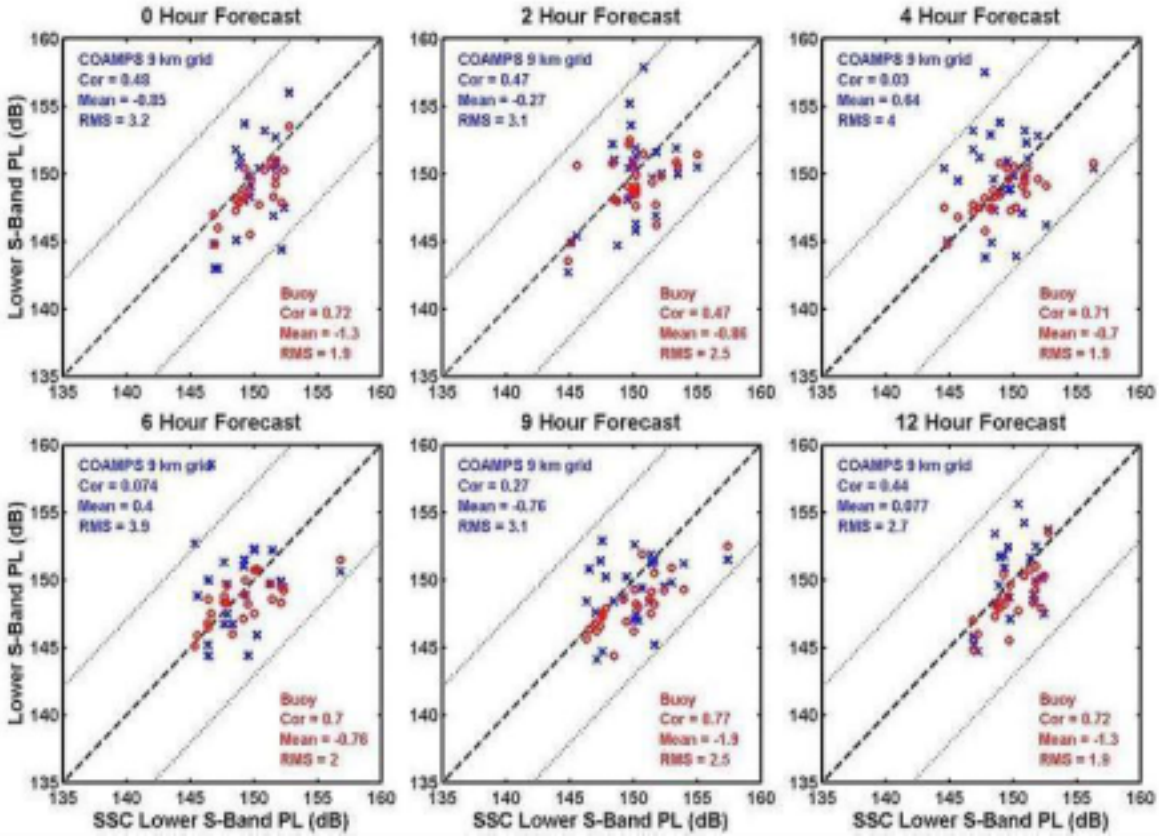

Figure 18. Same as Fig 17 except 9 km resolution COAMPS based data.

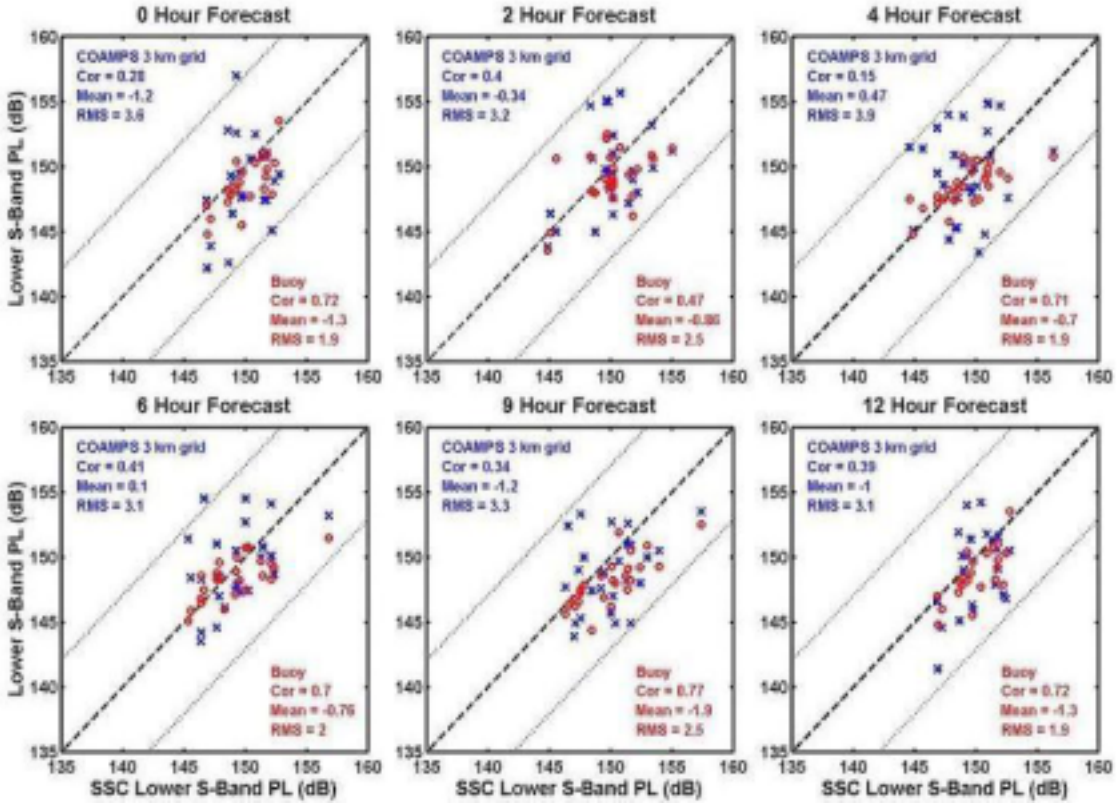

Figure 19. Same as Fig 17 except 3 km resolution based data.

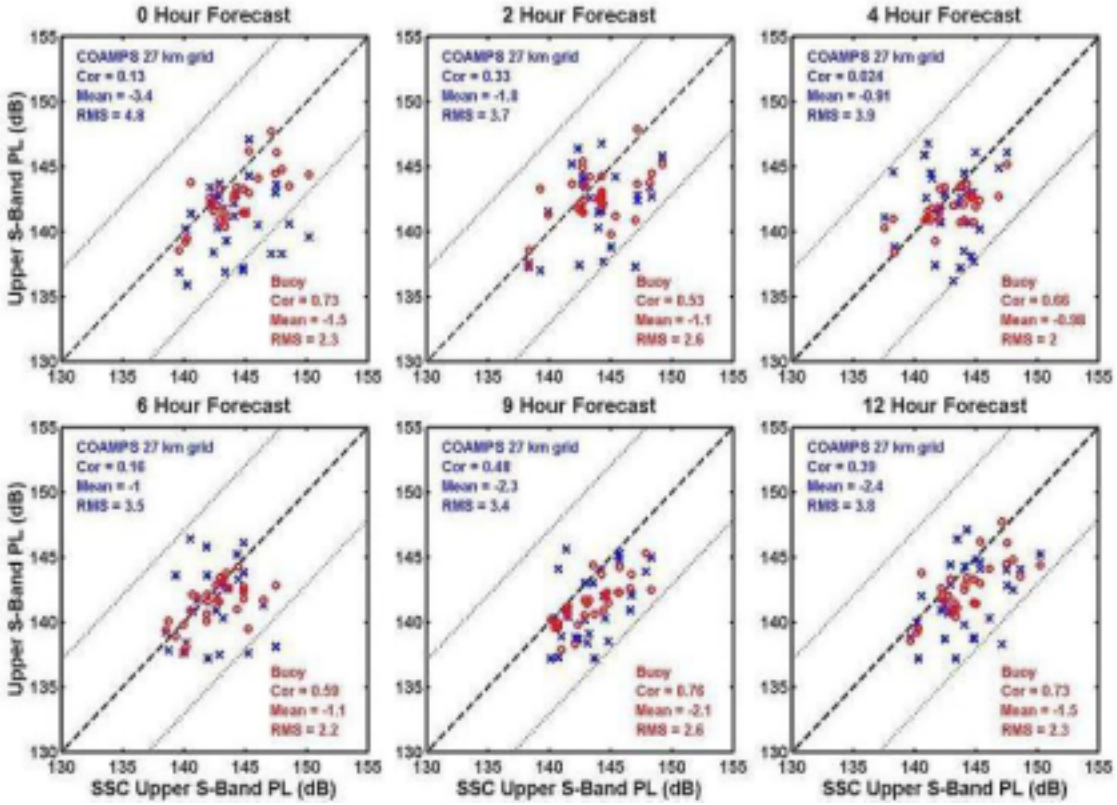

Figure 20. Same as Fig 17 (with 27 km resolution based data) except Upper level transmitter.

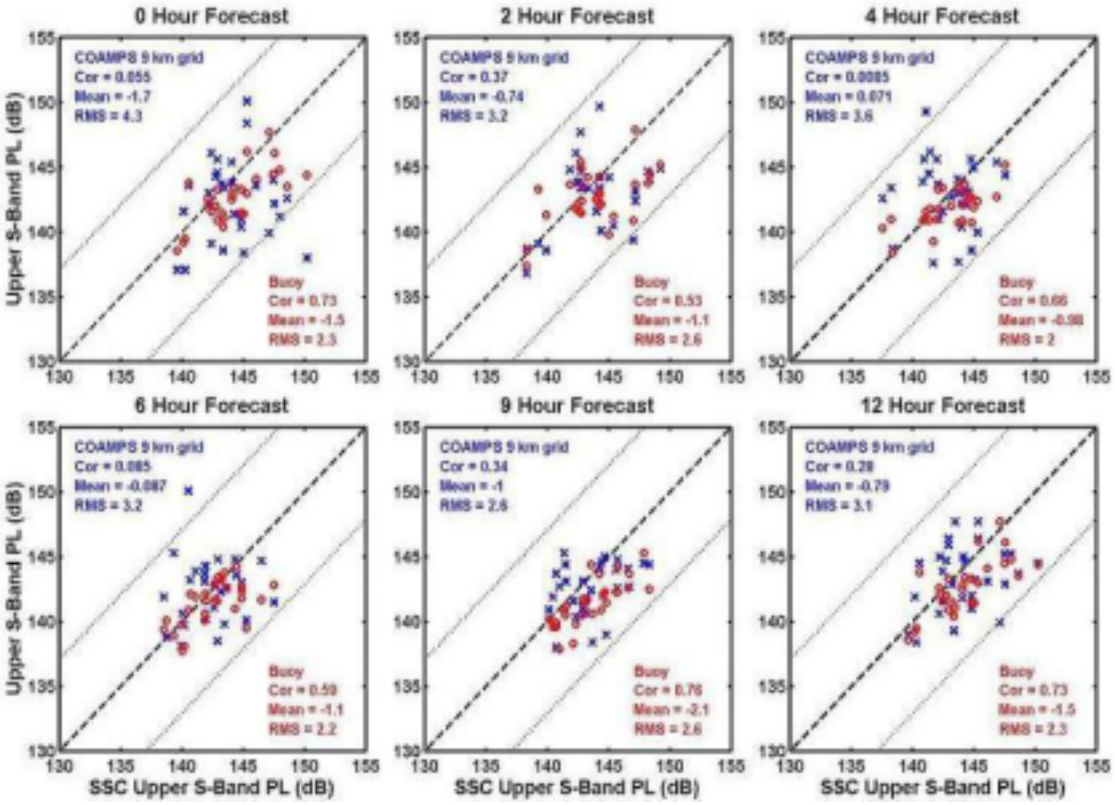

Figure 21. Same as Fig 20 except 9 km resolution COAMPS based data.

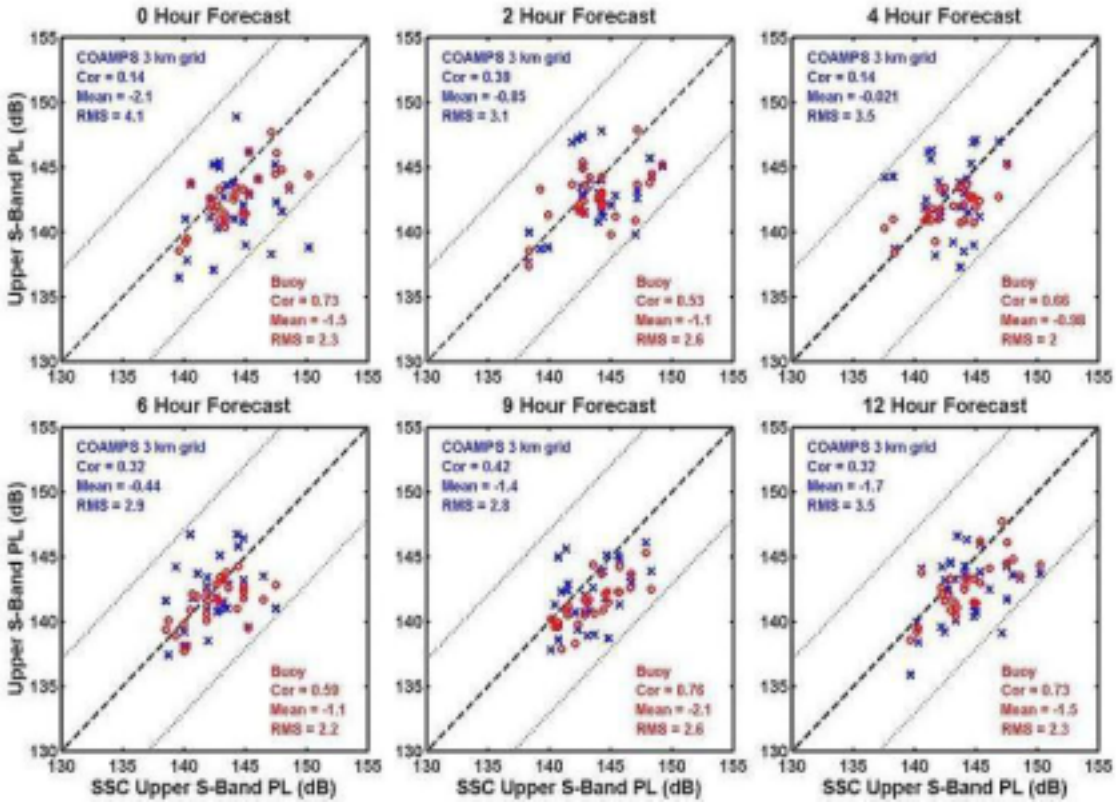

Figure 22. Same as Fig 20 except 3 km resolution COAMPS based data.

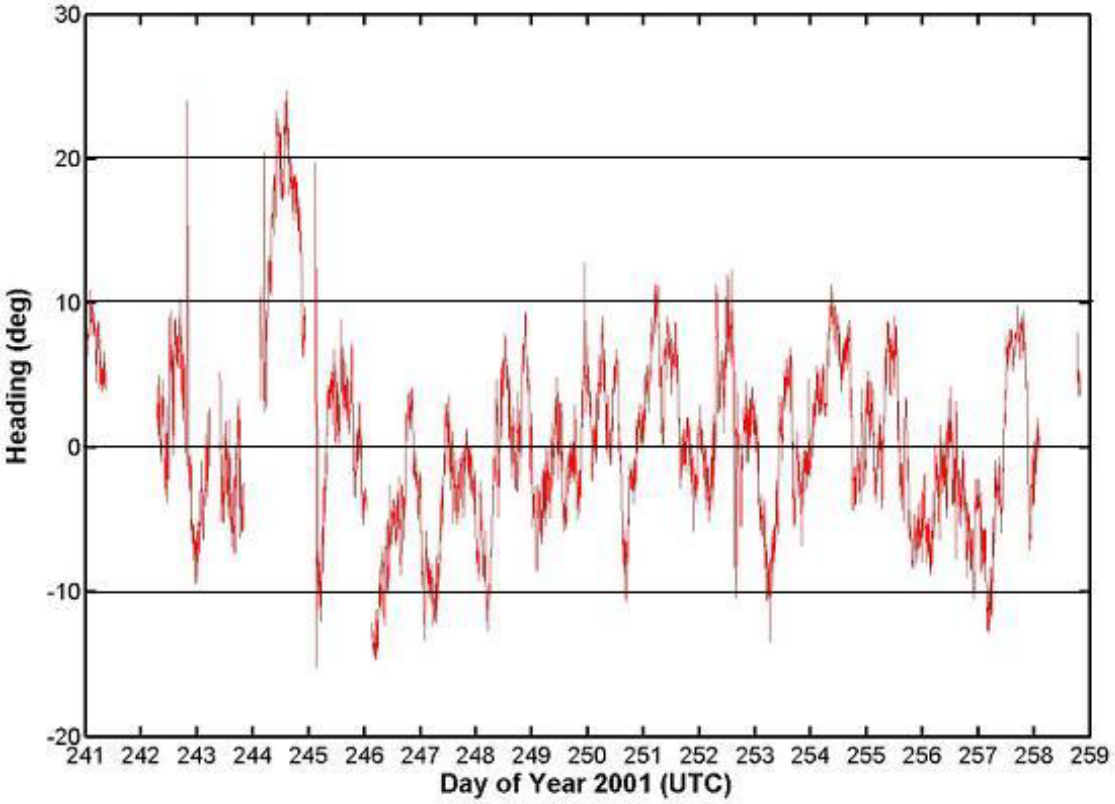

Figure 23. Time series of R/P FLIP's deviation from the desired heading (degrees).

THIS PAGE INTENTIONALLY LEFT BLANK

IV. ANALYSIS OF RESULTS

A. INTERPRETATION OF RESULTS

The purpose of this study was to examine the value of COAMPS model forecasts as input to the NPS bulk method evaporative duct model (and then to APM) to produce operationally useful propagation predictions. The results show that the COAMPS model METOC values are very similar to the in situ measured values at the NPS flux buoy. The impact of COAMPS resolution was examined and it was found that the coarser 27 km resolution model output is not as accurate as the 9 and 3 km, but it's still usable. This difference may be due to averaging differences (two vs. five vs. nine grid points averaged) rather than resolution. It's doubtful that one would see great improvement on the 3 or 9 km grid since the grid points used were over the open ocean and upstream of the island. With regard to overall predictions, long-term trends were well captured, but short-term small-scale variations were often missed. Over the short 12 hr forecast period, the comparisons of METOC and propagation loss values showed that initial/analysis output is the least accurate and there is no discernable decrease in forecast accuracy with time. The NPS model calculated EDH values from the buoy observations and COAMPS predictions are very similar overall with a mean RMS difference of slightly less than 2m. The buoy data based propagation loss predictions were found to be biased toward under predicting prop loss by ~1dB and produced a mean RMS error of just over 2 dB compared to the measured prop losses. The COAMPS model output-based prop loss values showed less bias and a slightly greater mean RMS error (~3dB).

Studies based on AEGIS ship self-defense requirements suggest that that propagation prediction within 3-5 dB is of significant operational value (Dockery 1997). It would therefore be easy to initially conclude that this study provided a quite valuable set of results since, by following the basic methodology of this study, it would leave the war-fighter confident in the resulting radar propagation predictions. Unfortunately such a conclusion would be misleading if it applied without some interpretation based on location of and general conditions for the following reasons: the environment during RED was very consistent and was always slightly unstable, SST>Tair by 1 or 2°C. The

combination of these two factors reduces the impact of the above conclusion as will be discussed in the following section.

B. ENVIRONMENTAL SENSITIVITY

An aspect of the RED data set was the exclusive occurrence of unstable conditions. Figure 24 illustrates typical situations in which the *m* profiles in unstable surface layers exhibit sharper curvature and have a much more well-defined minima in *m* and a lower evaporation duct height than in stable cases. The stable case exhibits very little change in *m* over most of the model's height domain. This demonstrates that small changes in the model input can have a large impact on the resulting evaporation duct height in stable conditions, as will be discussed below (Frederickson and Davidson 2003).

In Figures 25 and 26 evaporation duct heights computed by the NPS model are plotted versus the air–sea temperature difference (ΔT) for different relative humidity and wind speed values, as indicated. From these plots we can make the following observations regarding the general behavior of the NPS bulk method evaporation duct model under different environmental conditions:

In general the model exhibits much more complex behavior and much larger variations in evaporation duct height values in stable conditions ($\Delta T > 0°$ C) than in unstable conditions ($\Delta T < 0°$ C). This is especially true at lower wind speeds and relative humidity values.

The evaporation duct height generally increases as relative humidity decreases (except over a narrow range of conditions with low winds and small positive air-sea temperature differences). This behavior is expected because with a lower value of RH the humidity, and therefore *m*, decreases faster with height from its near-saturation value at the surface, leading to a higher elevation at which $dm/dz = 0$. For a given change in relative humidity the resulting evaporation duct height difference is generally much larger in stable conditions ($\Delta T > 0°$ C) than unstable conditions ($\Delta T < 0°$ C).

The evaporation duct height estimates are generally much less sensitive to variations in the model input parameters (U, T_{air}, T_{sea}, RH) in unstable conditions than

stable conditions. This means that measurement errors in the model input parameters will most likely result in larger evaporation duct height and refractivity profile errors in stable conditions than in unstable conditions.

For stable conditions the shape and hence, the evaporation duct height, would be quite sensitive to COAMPS predicted quantities. This is clearly indicated on the right hand sides, Tair>SST, of the panels in Figures 25 and 26.

C. SENSITIVITY ANALYSIS

The adequacy of COAMPS predicted values for estimating propagation loss depends on the sensitivity of the evaporation duct profile to changes in the predicted METOC parameters. In unstable conditions with ΔT less than $-1°$ C, the EDH errors resulting from typical input uncertainties of +/- 1 m/s WS, 3% RH, and 1°C SST and Tair are very similar for all four parameters (WS, RH, SST and Tair) and are less than 1 m in every case. In this regime the model can be considered to be relatively insensitive to input errors. The estimated total errors in EDH, due to all the input uncertainties combined, are less than 1 m for all humidity and wind speed conditions examined. This accuracy is quite suitable for high-fidelity propagation modeling and assessment.

For weakly unstable cases with $-1°$ C $< \Delta T < 0°$ C, the EDH errors due to uncertainties in the input parameters increase rapidly as ΔT approaches 0. This is because within this region the model is transitioning from the unstable profile functions to the stable functions. EDH errors within this regime can become very large at low wind speeds.

In weakly stable conditions with $0°$ C $< \Delta T < 1°$ C, the typical EDH errors increase dramatically as the air-sea temperature difference increases, especially for lower relative humidity and wind speed values.

In strongly stable conditions with $\Delta T > 1°$ C the EDH errors exhibited the following behavior: EDH errors tend to decrease as the wind speed increases; EDH errors increase with decreasing relative humidity; the model is extremely sensitive to input

errors, especially at low wind speeds and low humidity; the larger errors seen in stable conditions are due in part because the *m* minimum in vertical profiles in stable conditions is not as well defined

D. ERRORS DUE TO THE MODEL ASSUMPTIONS

In addition to uncertainties in the model input METOC parameters the accuracy of the derived bulk evaporation duct model profiles is directly related to the extent that each assumption the model is built upon is valid for the current environmental conditions. In other words, each simplifying assumption incorporated into the model introduces an additional potential source of error in the resulting modified refractivity profile and evaporation duct height estimates.

Possible sources of error include the following: the atmospheric conditions are not stationary and/or are not horizontally homogeneous, as required by MOS theory; the turbulent fluxes are not nearly constant with height, as required by MOS theory; the actual vertical temperature and humidity profiles depend upon additional parameters than those included in traditional MOS theory (u_*, θ_*, q_*, z and g/θ_v). Examples of such additional parameters could possibly include wave age, fetch, internal boundary layer height, etc.; there are uncertainties in the model's empirically determined constants and functions (Φ_U, Φ_θ, k, α, R_θ, etc.).

It is important to understand that the bulk model is empirical and was formulated and essentially 'calibrated' for open ocean applications and implicitly assumes fully developed, deep-water wave conditions. Therefore, the model may not perform as well for coastal locations, especially with off-shore winds, since the surface wave field is more likely to not be fully developed because of short fetch and shoaling effects. In addition, departures from MOS theory and invalid model results are more likely to occur with off-shore flow in coastal regions due to non-stationary and non-horizontally homogeneous conditions caused by the advection of land-influenced atmospheric properties over the ocean and the possible formation of internal boundary layers as air parcels are advected over the ocean with its contrasting surface characteristics.

The EDH was used as the METOC reference for refractive conditions in this study and will continue to be the reference in operational assessment of effects. The

influence of EDH variations on radar propagation, whether due to actual atmospheric changes or model prediction errors, can be quite complex because they depend on so many different factors. These include the transmitter height, the radar wave frequency, the exact range and height of interest, and stability-dependent refractivity profile shape differences for a given EDH. The latter is quite important and has led to the use of the predicted profile versus the EDH in propagation loss models. Because of the complex relationships between these multiple factors, it is difficult to devise simple 'rules of thumb' to describe the changes in propagation resulting from EDH variations. The simplest rule is that propagation differences generally increase with increasing EDH variations.

For example, a one meter EDH variation in unstable conditions may result in larger propagation changes than a 1 m EDH variation in stable conditions, because in unstable conditions the profiles tend to exhibit sharper minima, whereas in stable conditions the profiles have less curvature and the *m* minimum is not as sharply distinguishable. The propagation changes due to EDH variations are usually larger when the transmitter antenna is located within the duct as opposed to above the EDH. Propagation changes will also be greater for higher frequencies because they are more affected by the evaporation duct. It should be kept in mind that the evaporation duct height is a representative parameter for describing refractive conditions above the ocean surface and that near-horizon radar propagation depends upon a complete description of the vertical *m* profile shape throughout the surface layer.

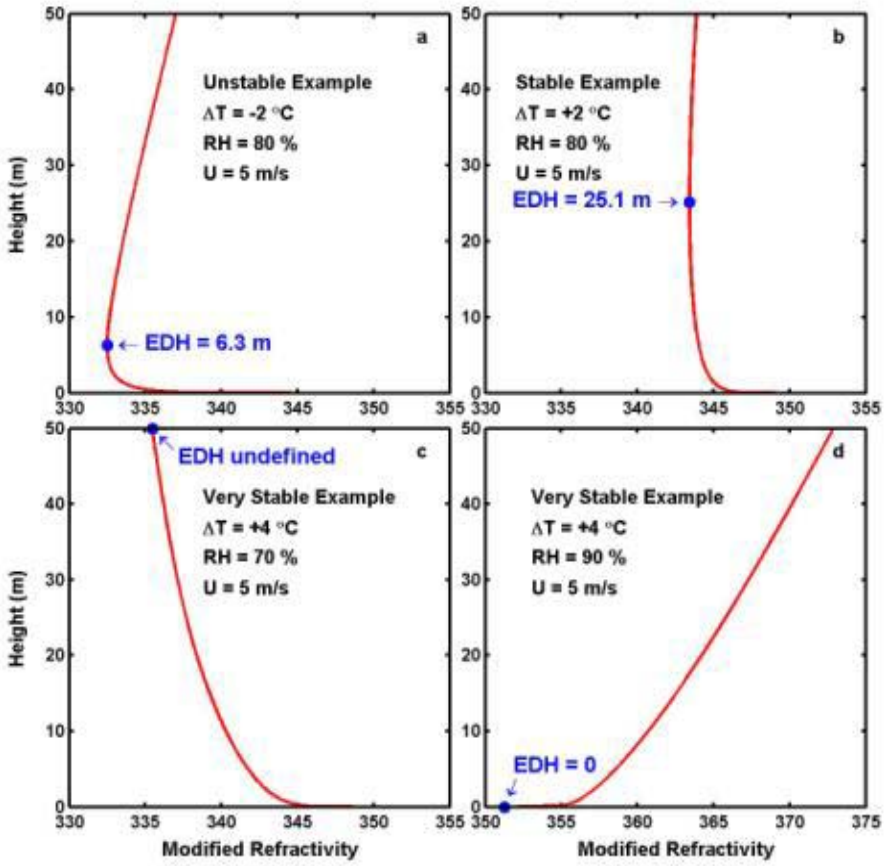

Figure 24. Plots of vertical *m* profiles computed by the NPS bulk evaporation duct model for four environmental conditions: a) Unstable conditions with Tair-SST difference of -2°C; b) Stable conditions with Tair-SST difference of +2°C and 80% RH; c) Very Stable conditions with Tair-SST of +4°C and 70% RH; d) Very Stable conditions with Tair-SST of +4°C and RH of 90%.

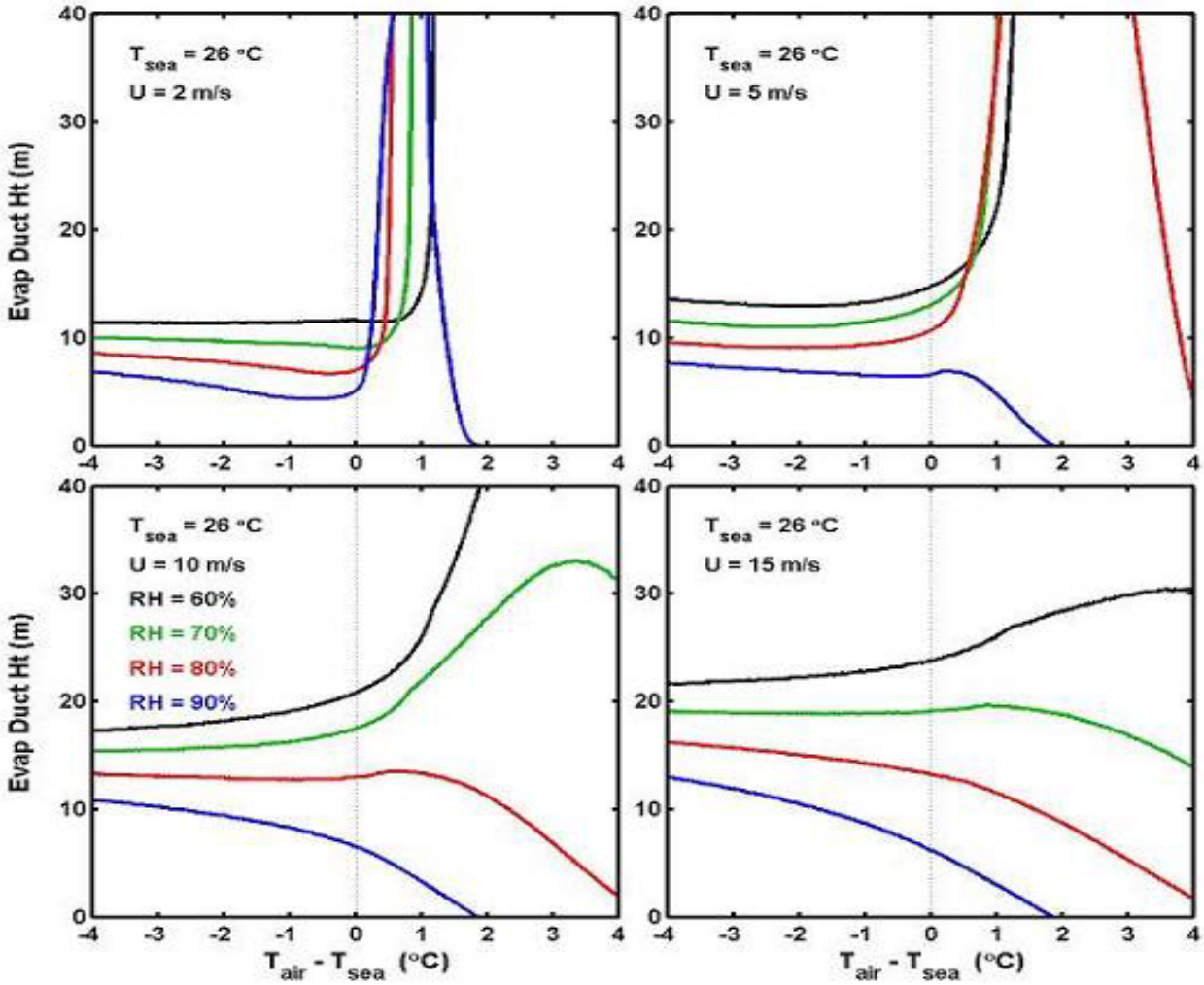

Figure 25. Evaporation Duct Heights computed by the NPS bulk evaporation duct model plotted vs. Tair-SST (°C) for various RH and WS as indicated.

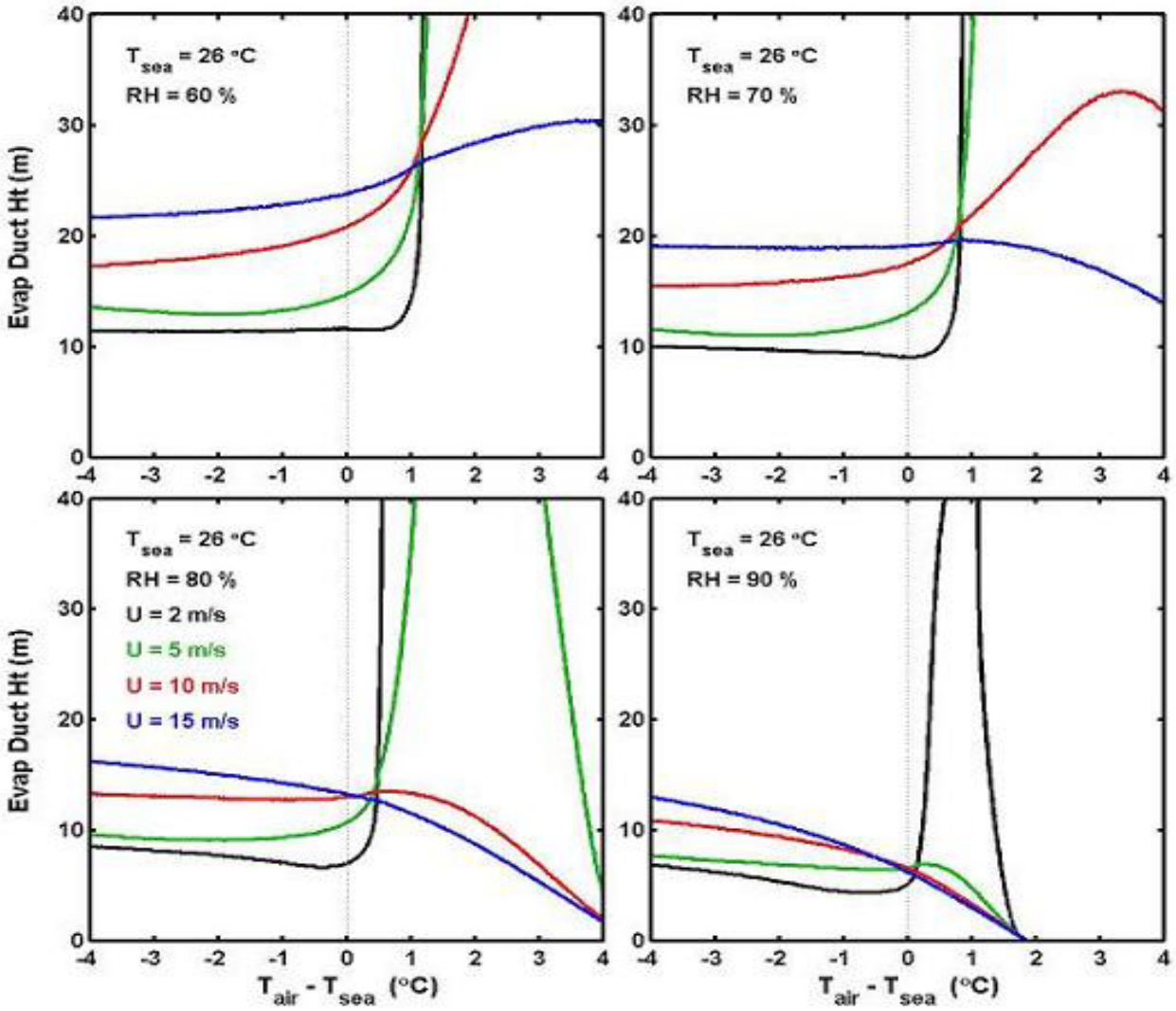

Figure 26. Evaporation Duct Heights computed by the NPS bulk evaporation duct model plotted vs. Tair-SST (°C) for various RH and WS as indicated.

V. CONCLUSIONS

With consideration given to the previously presented interpretation of results relative to sensitivity analyses, the results of this study are very promising. In the RED conditions, COAMPS forecasts performed very nearly as well as the real time in situ measurements, which is truly impressive. The resulting propagation loss forecasts were easily accurate enough to be of significant operational usefulness, i.e. < 5 dB. As discussed, however, the RED conditions were not difficult to predict for. Further, conditions affecting electromagnetic propagation through this type of atmosphere are not sensitive to small changes in the COAMPS predicted METOC parameters that are used as input for the NPS bulk evaporation duct model. As long as the air-sea temperature difference is slightly negative (unstable conditions) it is easy to get good results. Also, it is important to understand that electromagnetic propagation can be significantly altered by small-scale short-term variability which METOC models are not capable of predicting due to model physics errors, parameterizations, and assumptions, resolution limitations, and possibly most importantly, observational data sparseness.

A. AREAS NOT ADDRESSED OR REQUIRING FURTHER STUDY

There are many areas of this study that deserve further investigation. The most obvious direction for further investigation is the study of COAMPS model performance and the resulting propagation predictions in more varied environments including stable, neutral, and unstable conditions. This study did not "flex" COAMPS prediction. The study needs to be extended to more complex and varied weather. During this study there were no significant changes in the weather conditions or patterns. It is necessary to verify COAMPS's value in a location where there are warm and cold fronts moving through the area; topographic effects are prevalent; tropical storms effect the environment; etc.

The lowest sigma level COAMPS model output (at 10m) was used in this study for the Tair, Pres, Water Vapor, and WS, along with the SST field data , which were used to create the *m* profiles. The COAMPS SST field is unchanging, which could lead to large errors in environments that are close to neutral. There may be a better model to

use for the SST input. The NPS bulk model can use any METOC parameters from heights less than 50m. The second lowest sigma level (at 35m) could have been used for input as well, and may yield better or worse results. Additionally, COAMPS, which estimates surface layer properties based on MOS parameterization, predicts the flux-profile relationship determining U*, T*, and Q* values directly. These were not available for this study but could be used as input into the NPS model and may improve the propagation predictions.

A necessary direction for further study is to determine how well COAMPS performs with forecasts of greater than 12 hours. Due to the model runs available for this study, it can only be concluded that forecasts of up to 12 hours perform well enough to be beneficial in propagation prediction. This leads to a necessary examination of the relative value of 24, 36, 48-hour or even longer forecasts. There is no question that for planning purposes, an accurate 72-hour propagation prediction would be valuable to the war-fighter.

LIST OF REFERENCES

Babin, S. M., G. S. Young, and J. A. Carton, 1997: A new model of the oceanic evaporation duct. *J. Appl. Meteor.*, 36, 193-204.

Bean, B. R., and E. J. Dutton, 1968: *Radio Meteorology*. Dover Publications, New York, 435 pp.

Buck, A. L., 1981: New equations for computing vapor pressure and enhancement factor. *J. Appl. Meteor.*, 20, 1527-1532.

Davidson, K. L., 2002; Assessment of atmospheric factors in EM/EO propagation, *Class Notes for MR4416, Naval Postgraduate School, Monterey, CA*.

Dockery, G. D., 1997: Meteorological data requirements for assessment of AEGIS air defense capability. Electromagnetic/Electro-Optics Prediction Requirements & Products Symposium Proceedings*.,* 111-119.

Easton, R. C., and E.R. Sanabia, 2000, "Exploiting the Environment to Win in the 21st Century," White Paper: USS PORT ROYAL (CG-73), 17 pp.

Fairall, C. W., K. L. Davidson, G. E. Schacher, and T. M. Houlihan, 1978: Evaporation duct height measurements in the mid-Atlantic. Naval Postgraduate School Report NPS61-78-005, 101 pp.

Fairall, C. W., E. F. Bradley, D. P. Rogers, J. B. Edson and G. S. Young, 1996: Bulk parameterization of air-sea fluxes for Tropical Ocean-Global Atmosphere Coupled-Ocean Atmosphere Response Experiment. *J. Geophys. Res.*, 101, 3747-3764.

Frederickson, P, A., and K. L. Davidson, 2003: An operational bulk evaporation duct model. *Draft,* 1-51.

Goldhirsh, J., and G. D. Dockery, 1994: Lateral resolution considerations for refractivity profiles associated with remote sensing measurements of over-water coastal regions. *NATO Advisory group for Aerospace Research and Development (AGARD) Conference Proceedings,* 11.1-11.13.

Goroch, A. K., M. S. Jordan, P. A. Frederickson, and K. L. Davidson, 2000: Standard meteorological equations and algorithms used in MORIAH processing. Naval Research Laboratory Report, Monterey, CA, 26 June, 103 pp.

Hodur, R. M., 1996: The Naval Research Laboratories Coupled Ocean/Atmospher Mesoscale Prediction System (COAMPS). *Monthly Weather Review,* 125, 1414-1430.

Patterson, W. L., 1985: Comparison of evaporation duct and path loss models. *Radio Sci.*, 20, 1061-1068.

Paulus, R. A., 1985: Practical application of an evaporation duct model. *Radio Sci*., 20, 887-896.

INITIAL DISTRIBUTION LIST

1. Defense Technical Information Center
   Ft. Belvoir, VA

2. Dudley Knox Library
   Naval Postgraduate School
   Monterey, CA

3. The Oceanographer of the Navy
   United States Naval Observatory
   Washington, DC

4. Prof. Kenneth L. Davidson, MR/DS
   Department of Meteorology
   Naval Postgraduate School
   Monterey, CA

5. CAPT C. R. Gunderson, CO
   FNMOC
   Monterey, CA

6. Dr. Robert E. Gover, Code 5753.00
   Naval Research Laboratory 3310
   Washington D.C.

7. G. Daniel Dockery
   The Johns Hopkins University/Applied Physics Laboratory
   Johns Hopkins Road
   Laurel, MD

8. Richard Paulus
   SPAWARSYSCEN-SD, 2858
   San Diego, CA

9. J. Stapleton, Code T44
   Naval Surface Warfare Center, Dahlgren Division (NSWCDD)
   Dahlgren, VA

10. CAPT Robert L. Clark
    Space and Naval Warfare Systems Command (PMW-155)
    San Diego, CA

11. Thomas Piwowar, PMW
Space and Naval Warfare Systems Command
San Diego, CA

12. Kenneth Anderson
SPAWARSYSCEN-SD, 2858
San Diego, CA

13. Paul Tiedeman
Naval Sea Systems Command
Washington, DC

14. Dr. Stephen Burk
Naval Research Laboratory
Monterey, CA